Chapter 3
Anisotropic Gold Nanoparticles: Preparation, Properties, and Applications

Chenming Xue and Quan Li

Abstract Anisotropic metal nanoparticles with a catalog of promising anisotropic electronic, optical, and chemical properties have been regarded as enabling building blocks in the bottom-up fabrication of functional materials and devices. Specifically, anisotropic gold nanoparticles are currently emerging as fascinating materials due to their unique shape-, size-, and surface-dependent properties. In this chapter, we present the synthesis, properties and applications of different one-, two- and three-dimensional anisotropic gold nanoparticles (AuNPs). The most widely adopted top-down and bottom-up synthesis approaches have been discussed in addition to some of the recently introduced new methods for the fabrication of differently shaped anisotropic AuNPs. The optical property, photothermal effect, surface enhanced Raman scattering, fluorescence enhancement and quenching, surface modification, toxicology, and supramolecular organizations of anisotropic AuNPs have been highlighted. Various practical and potential applications of anisotropic AuNPs in catalysis, sensing, photothermal therapy, drug and gene delivery, and biological and biomedical areas are briefly outlined.

3.1 Introduction

Since medieval period, gold nanoparticles (AuNPs) have been used to decorate church glasses and Lycurgus cup [1]. However, they were beyond comprehension due to the then scientific limitations. In the early part of 20th century, scientists began to investigate these extremely small particles, and several theories were developed to explain their unusual and unique physical properties compared to the bulk materials. For example, the famous Mie theory [2] of which the most special one is localized surface plasmon resonance (LSPR), e.g. the free electrons trapped

C. Xue · Q. Li (✉)
Liquid Crystal Institute and Chemical Physics Interdisciplinary Program,
Kent State University, Kent, OH 44242, USA
e-mail: qli1@kent.edu

Q. Li (ed.), *Anisotropic Nanomaterials*, NanoScience and Technology,
DOI 10.1007/978-3-319-18293-3_3

in the particle surface show the collective oscillation (Fig. 3.1) frequency, resulting in a plasmon absorption band in the visible to near infrared (NIR) and even to infrared (IR) region. A solution of well-dispersed AuNPs shows a typical deep-red color [3]. In the past decades, the AuNPs were systematically studied, nevertheless sophisticated synthesis methods and attractive applications based on their unusual properties are under intensive investigation. In this context, the spherical (isotropic) AuNPs are so far the most studied class of metal nanoparticles.

In contrast to isotropic AuNPs, anisotropic AuNPs have caught a broad interest due to their appealing and unprecedented properties. The existence of anisotropic AuNPs was noticed in the beginning of the twentieth century by Zsimondy, who discovered colored solutions of anisotropic AuNPs. He also invented the ultramicroscope to visualize the shapes of gold particles, and received the 1925 Nobel Prize for "his demonstration of the heterogeneous nature of colloidal solutions and for the methods he used". It was not until the past decade that anisotropic AuNPs became a research endeavor at its own right and has been drawing great attention because the structural, optical, electronic, and catalytic properties are different from, and most often superior to those of spherical AuNPs. All these fascinating applications are based on their size- and shape-dependent electronic and optical properties that also vary in individual state and self-assembled state. For example, isotropic AuNPs exhibit one relatively simple LSPR, while anisotropic gold nanorods (AuNRs) exhibit two LSPR signals: longitudinal (along the long axis) and transverse (across the long axis) LSPR (Fig. 3.1b). Owing to their unusual properties, anisotropic AuNPs have qualified for broad and interesting applications in different areas such as sensors, biological and biomedical treatments, optical devices and metamaterials.

During the past two decades, the explorations of anisotropic AuNPs including their properties and applications have become accessible and been extensively expanded. The anisotropic AuNPs show interesting light absorption and scattering phenomena, resulting from extraordinary shape dependent collective electronic resonances. According to their anisotropic shape and self-assembled state, they can absorb light from visible to IR region. For example, depending on the AuNRs' tunable aspect ratio (length/diameter), the longitudinal LSPR varies from visible frequency (small aspect ratio) to NIR and even IR frequencies (large aspect ratio). The wavelength region between 800 and 1300 nm, the so-called "biological window" can penetrate tissue and cells without causing cell damage. Moreover, the self-assemblies of AuNRs can further alter LSPR due to plasmon coupling between neighboring AuNRs. Based on these unusual plasmonic effects of anisotropic AuNPs, they show attractive properties such as light absorption and scattering, fluorescence, photothermal effect, and optical tuning, leading to promising applications in medicinal diagnostics and photothermal therapy ("theranostics") [4–7], and optical devices [8].

The fabrications of anisotropic AuNPs are based on two different well-developed methods: top-down physical nanofabrication approach and bottom-up wet chemistry approach. Both approaches have their own pros and cons. The top-down methods are easy to produce AuNPs in a well-organized fashion and with controlled narrow size distribution, but the sizes are usually relatively large. The bottom-up

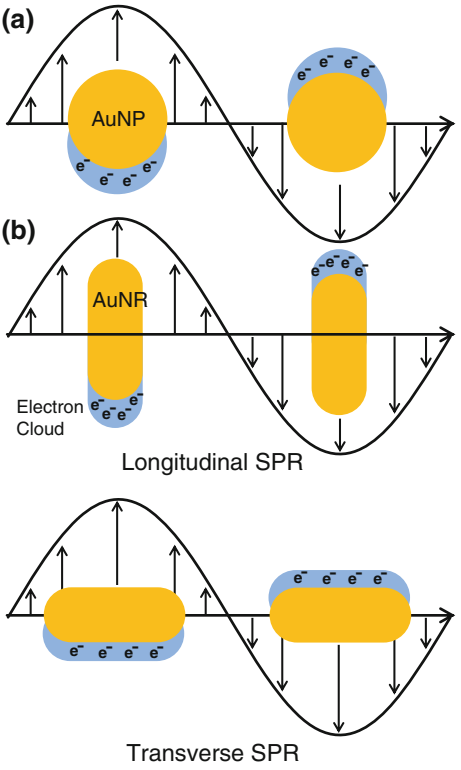

Fig. 3.1 Schematic depictions of the LSPRs of **a** isotropic AuNP and **b** anisotropic AuNR

wet-chemistry methods have advantages in preparing small size colloidal AuNPs with good yields and controllable polydispersity. However, organizing them into well-ordered arrays is challenging. For the chemistry methods, during the past two decades scientists have discovered and improved the seed-mediated growth method to prepare AuNPs with high efficiency and excellent size distribution. This method is very successful in synthesizing AuNRs, the most representative anisotropic AuNPs. There are also other wet-chemistry synthesis methods, e.g. photochemistry, electrochemistry, sonochemistry, templates, galvanic replacement, for anisotropic AuNP synthesis. With these methods, fascinating shapes of anisotropic AuNPs including one-dimensional (1D) (nanowires, nanotubes, and nanobelts), two-dimensional (2D) (stars, pentagons, squares/rectangles, dimpled plates, hexagons, and truncated triangles), and three-dimensional (3D) (nanotadpoles, nano-urchins, nanodentrites, nanocubes and core-shell structures) have been realized.

It is interesting to note that anisotropic AuNPs show special properties according to their different shapes such as optical property, photothermal effect, surface-enhanced Raman scattering (SERS) effect, fluorescence enhancement and quenching phenomena, toxicology, and self-assembly behaviors. Surface coating is an important issue after synthesis, providing stability as well as compatibility. Especially for biological and biomedical applications, it is utmost important to

passivate the surface of nanoparticles with biocompatible groups in order to introduce AuNPs into biosystem for functionalization and to provide necessary intermolecular interactions to combine AuNPs with demanding materials for drug delivery or gene transfer. Furthermore, anisotropic AuNPs have shown other interesting applications in diverse areas such as catalysis, sensing and molecular recognition, nanoelectrodes and optical tuning.

Although anisotropic AuNPs are relatively new building blocks, they have become a rapidly emerging research field due to their promising applications. This chapter covers an overview of this interesting research subject. Various synthesis approaches for preparing and stabilizing anisotropic AuNPs with an emphasis on the representative and most commonly used seed-mediated wet-chemistry approach are introduced. The typical properties of different anisotropic AuNPs are highlighted based on the AuNPs' morphology and supramolecular assemblies. Finally, the functionalization and attractive applications of the anisotropic AuNPs in optics, photonics, catalysis, materials science, biological and biomedical areas are presented.

3.2 Methods and Techniques for Synthesis of Anisotropic Gold Nanoparticles

3.2.1 Top-Down Method

Top-down physical lithography methods are direct ways to produce anisotropic AuNPs, which have typical polycrystalline structures. Among them, the most widely used method is electron-beam lithography (EBL) [9]. In the typical procedure, an electron-sensitive resist is initially coated on the substrate. Followed by the exposure to an electron beam, the area will dissociate into smaller polymer segments that can be selectively removed by washing with a developing agent. Then, gold can be deposited onto the opening patterns written by the electron beam. This lift-off technique can offer anisotropic AuNPs with controllable shapes and sizes in tens of nanometers' length-scale. Focused ion beam (FIB) lithography [10] is another lithography technique which sputters away unwanted portions of a continuous film by a raster ion beam (typically gallium), creating nanostructures of the desired shapes. Anisotropic AuNPs have been produced using both EBL [10] and FIB techniques [11]. FIB produced Au nanodisks [12]. EBL and FIB techniques were also combined to prepare anisotropic AuNPs arrays of Au microholes [13], grooves, nanowire circuits [14], hexagonal arrays of Au triangles [15] and Au nanorings [16]. Mirkin's group has discovered another lithography method called on-wire lithography (OWL) [17, 18], which can make gapped cylindrical structures on a solid support with gaps and segment length controlled on a length scale under 100 nm by the template-based electrochemical process (Fig. 3.2) [19]. Although the top-down lithography techniques can produce AuNPs with controllable size, shape, and alignment, their scaling up is limited and smaller AuNPs with sizes less than 10 nm are not easily accessible.

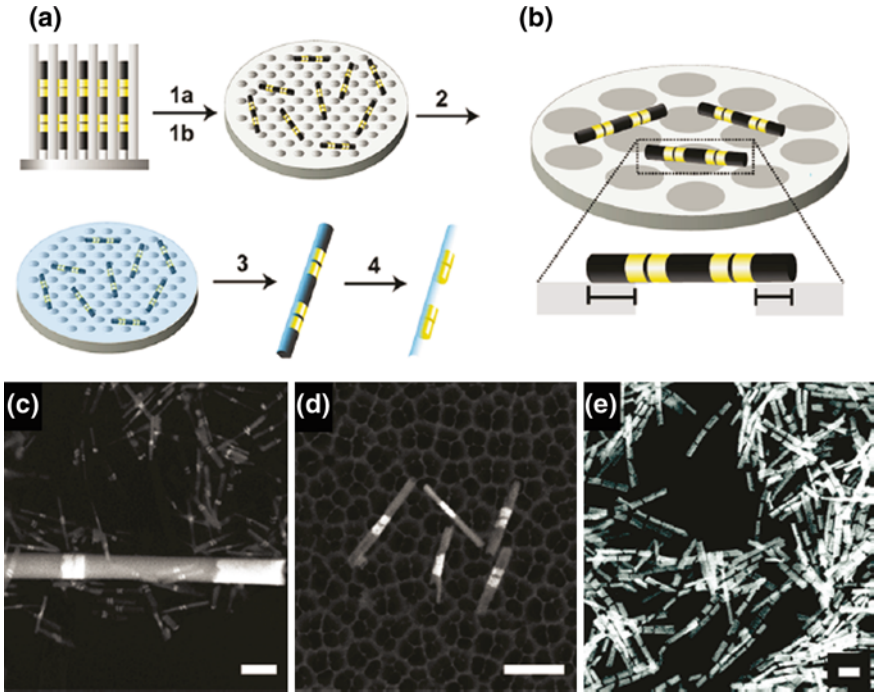

Fig. 3.2 Synthetic strategy for preparing sub-100 nm diameter nanostructure arrays with on-wire lithography (OWL). **a** Schematic depiction of method beginning with (1a) release of template-synthesized multisegmented metal nanowires from anodic aluminum oxide (AAO) membranes into solution by dissolving the membrane and metal backing. (1b) Vacuum filtration of nanowires on to larger pore AAO membranes. (2) Electron beam evaporation of a thin (5–10 nm) SiO_2 backing layer (*blue* coating). (3) Sonication in ethanol to release half-coated wires into solution. (4) Selective etching of sacrificial material (typically Ni, black segments) to produce 1D nanostructure arrays with geometry matching the original nanowire. **b** Schematic showing the decreased interaction area (*solid black lines*) between the nanowires and the porous substrate, decreasing the van der Waals attraction between the surfaces. **c–e** SEM images of 55 nm Au–Ni nanowires after steps 1, 2, and 4 (**c**, **d**, and **e**, respectively). **c** The 55 nm diameter Au–Ni nanowires codeposited with 270 nm Au–Ni nanowires, highlighting the increased resolution available with this new method compared to the previous smallest OWL structure. Scale bar is 350 nm. **d** Au–Ni nanowires filtered on to a porous AAO substrate, depicting the decreased interaction area shown schematically in (**b**). Scale bar is 300 nm. **e** SEM image of 55 nm Au nanorods arrays with varying gap sizes after etching away the Ni segments. Scale bar is 165 nm [19]. Copyright 2011 American Chemical Society

3.2.2 Bottom-Up Method

To prepare anisotropic AuNPs, the bottom-up solution based method has been well developed and widely used. The simplest and most easily accessible 1D anisotropic AuNRs have drawn great attention from scientists. Conditions of seed-mediated growth method, photochemistry, electrochemistry, sonochemistry, templates,

galvanic replacement have been discovered and developed. During the earlier research, different methods have been attempted to produce anisotropic AuNPs. In early 1960s, vapor−liquid−solid (VLS) method has been demonstrated [20]. In 1989, Wiesner and Wokaun reported the first example of AuNRs by adding Au seeds into the solution of $HAuCl_4$. The seeds were created by reduction of $HAuCl_4$ with phosphorus (as in Faraday's synthesis) and these seeds further grew up to AuNRs by reduction of Au^{3+} with H_2O_2 [21]. Until 1990s, seed-mediated growth approach for AuNRs was discovered and after continual improvement, it has become the method of choice [22]. It offered a convenient and versatile wet-chemistry way to synthesize AuNRs with excellent yield, monodispersity and controllable aspect ratio and size, and also reproducibility. A typical procedure is shown in Fig. 3.3. Accompanying the progress of this seed-mediated growth method that provides feasible access to AuNRs, fundamental optical properties were recognized. AuNRs with the sizes of ~150−180 nm × 25 nm (length × width), which exhibit the aspect ratio between 8 and 20, have been synthesized [23]. It is worthwhile to mention that the modifications from the El-Sayed research group improved the yield and polydispersity of the AuNRs by replacing sodium citrate with the stronger cetyltrimethylammoniumbromide (CTAB) stabilizer during the formation of the seeds, as well as using $AgNO_3$ to

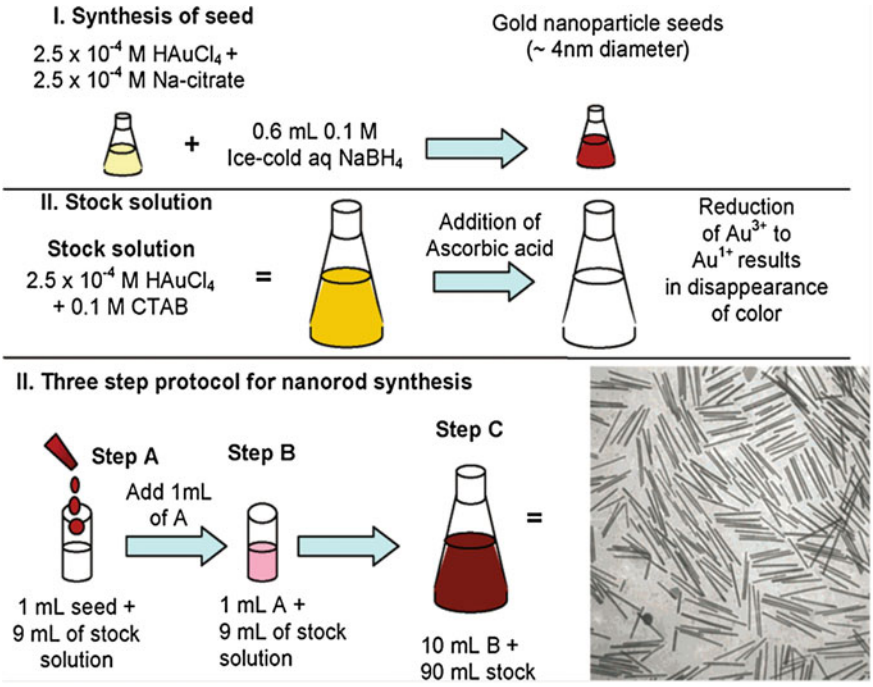

Fig. 3.3 Three-step seed-mediated growth approach for making gold and silver nanorods with a controlled aspect ratio [29]. Copyright 2005 American Chemical Society

direct the formation and to control the aspect ratio of the AuNRs [24]. The role of Ag^+ is also critical in formation of other shapes of AuNPs, for example, high-index concave cubic Au nanocrystals have been synthesized by the reduction of $HAuCl_4$ with ascorbic acid in the presence of a chloride-containing surfactant and small amounts of $AgNO_3$ [25]. The yield of such a procedure is about 99 % with aspect ratios between 1.5 and 4.5. Higher aspect ratios up to 10 or 20 were obtained upon the addition of a cosurfactant (benzylhexadecylammonium chloride (BDAC) [24] or Pluronic F-127 [26]) to the original growth solution and by varying the concentration of $AgNO_3$. The synthesized single crystal AuNRs have a penta-twinned structure with Au {111} lattice at the end-caps and the Au {100} or {110} along the longitudinal faces [27]. Besides, $AgNO_3$ has been found to play a critical role in the formation of long AuNRs [28].

AuNRs with low aspect ratio (aspect ratio: 2–5, size: ~20−60 nm × 12 nm) have been developed by a modified seed-mediated growth protocol [24, 30]. In this method, smaller AuNP seeds (ca. 1.5 nm) stabilized with CTAB are added to the growth solution with the assistance of a small amount of $AgNO_3$ and the mild reducing agent ascorbic acid. $AgNO_3$ used herein is crucial in controlling AuNR shapes. The AuNRs produced by this method display different crystal faces compared to the earlier ones [31]. Later, the seed-mediated growth procedure has been modified as a "seedless" version which uses small organic additives to control AuNR sizes and aspect ratios (between 2 and 5). In such a new way, the standard silver-assisted growth method is employed and seeds are generated in situ by adding a small amount of the strong reducing agent sodium borohydride, instead of using preformed AuNP seeds [32]. The control of aspect ratio is based on the sodium borohydride concentration rather than the $AgNO_3$ concentration. Interestingly, although the size of AuNRs (~25 nm × 6 nm) prepared through this "seedless" method is quite smaller than the formal procedures, the yield is poorer and the size distribution is broader.

Having been developed in the past years, the seed-mediated growth approach and its modified ones have become the most popular for synthesizing anisotropic AuNRs with aspect ratios from 2 to 20 with desirable yield and monodispersity. They have advantages of simple procedure, high yield, scale-up quantity, feasible size/shape control, and flexible for further structural modifications [33]. Similarly, AuNRs themselves can be used as seeds in the synthesis of more complex structures, for instance, Pt nanodots can form on AuNR surface which possesses more complex properties [34]. Based on this method, now commercially available AuNRs have appeared in market. This greatly promotes the research in anisotropic AuNPs and their fascinating applications.

With different additives (e.g. foreign metal ions, iodide ions), the overgrowth of colloidal AuNRs can be tuned affecting their shape, facet, aspect ratio and composition, e.g. forming dumbbell-like AuNR nanostructures [35]. Shape transformation from rod to octahedron is observed under sonication in dimethylformamide (DMF) in the presence of poly(vinylpyrrolidone) (PVP) [36]. Similarly, overgrowth of AuNRs can induce nanopeanut and octahedra structures by glutathione and cysteine [37].

However, the mechanism of AuNR growth during synthesis is one unsolved challenge to date. Even though large efforts have been devoted to this subject, it is still not fully understood. Fixing this can improve the efficiency and versatility of the synthesis of AuNRs in the future [38]. Two AuNR growth mechanisms were brought up and studied [39]. The growth is governed either by binding the head group of a cationic surfactant to the {100} face of the AuNP seed preferentially, instead of the less-favored rod end [29], or by the electric field of the double layer between the positively charged seed and negatively charged $AuCl^{2-}$ on the CTAB micelle. Different from multiply twinned crystalline citrate-capped seeds growing into multiply twinned structures, single-crystalline CTAB-capped seeds lead to single-crystalline AuNRs with {110} faces on the side and {100} faces on the end. Ag deposits on the {110} sides faster than that on the {100} ends, and in this way the seeds grow into rods. A hybrid mechanism involving diffusion of $AuCl^{2-}$ on the CTAB micelles to CTAB-capped seed spheres resulting from electric-field interactions has been proposed by Murphy and co-workers. Silver ions preferentially deposit onto the {110} facets, where CTAB molecules are preferentially bound and providing bromide counter ions forming an AgBr solid layer thereon, which results in particle growth into AuNRs along the {110} direction. There is a critical $[Br^-]/[Au^{3+}]$ ratio around 200 that leads to the maximum aspect ratio of the AuNRs, however beyond such ratio, Br^- acts as a poison.

3.2.3 Other Methods

3.2.3.1 Photochemistry

Photoreduction was an alternative method for generating anisotropic AuNPs. For instance, UV light can reduce $HAuCl_4$ to form AuNRs with the aid of rod shaped cationic micelles. The pioneer work of this method was introduced in 1995 by Esumi et al. [40]. Different from the seed-mediated procedure where the micelle surfactant molecules stabilize a specific crystal face resulting in AuNRs, in the photoreduction procedure, Au^{3+} ions bound to rodlike cationic micelle surfactant molecules to form ion pairs. After excited by UV light with 235 or 300 nm [41], the Au^{3+} ions were reduced to Au^0. This process includes the aggregation of metal nuclei to form primary particles, and these particles assemble to form AuNRs resulting from the stabilization of a specific crystal face by surfactant micelles [42]. One prominent advantage of this photocatalyzed procedure is that high yield of AuNRs can be obtained in a single step [32], rather than the typical two-step seed-mediated growth method. In the presence of poly(vinylpyrrolidone) (PVP) and ethylene glycol [43], or TiO_2 colloids [44], the photochemical method could be used to synthesize other anisotropic AuNPs such as platelet-like shape with an asymmetric five-twinned structure and six-star shape.

3.2.3.2 Electrochemistry

The electrochemical method to produce AuNPs was first reported by Svedberg in 1921. During 1990s chemists modified the electrochemical reduction method using organic surfactant (CTAB) and porous aluminum oxide membrane templates for shape control [45], and arrays of AuNRs with micrometer scale dimensions ($\sim$100 nm by 100–200 μm) were created [46]. Those sizes are too large, but smaller AuNRs (60 nm × 12 nm) can be prepared with modified synthesis approach by using surfactant mixtures as soft templates [47]. In this approach, an Au plate anode and a Pt plate cathode were immersed into an electrolyte containing CTAB and co-surfactant tetradodecylammonium bromide (TOAB). Binding to the CTAB micelle, $Au^{3+}Br_4^-$ first formed from the Au anode due to electrolytic oxidation, and then migrated to the cathode and reduced to Au^0. By the assistance from Ag^+ cations from redox reaction between Au^{3+} and an Ag plate, AuNRs were formed with controllable aspect ratios. These AuNRs were separated from the cathode by sonication [47]. As shown by high-resolution transmission electron microscopy (HRTEM) and diffraction studies, AuNRs produced by this way are single crystals having no stacking faults, twins, or dislocations, with aspect ratios of 3–7 [48]. With the advantages of simplicity, efficiency and applicability, electrochemical method is continually developed for the synthesis of other anisotropic AuNPs, for example dendritic AuNPs [49]. The photochemistry and electrochemistry methods have limitations of expensive synthesis and significant amount of byproducts: spheres, rods, cubes, plate, and prisms AuNP mixtures.

3.2.3.3 Sonochemistry

Ultrasonication is another useful approach for the synthesis of small nanoparticle, which can control both their shapes and sizes by the use of surfactants and alcohols [50]. With this method, single-crystalline flexible Au nanobelts with a width of 30–50 nm and a length of several micrometers have been synthesized [51].

3.2.3.4 Template

One successful well-known template for the synthesis of AuNPs is silica nanospheres. Around such templating cores, Au layers can be coated. This powerful strategy allows the control over the size and thickness of the Au nanoshells by changing the reaction time and the concentration of the plating solution [52]. Anisotropic AuNRs were generated on substrates from colloidal solution using catalytic seed nanospheres to directly grow [53]. However, only 15 % of seeds are converted to rods while the rest seeds promoted a myriad of shapes including spherical, triangular and hexagonal. To improve this method, nanoporous track-etched polycarbonate or anodized alumina membrane was used as the templates where gold atoms are deposited by electrochemical reduction [54]. To tune the

AuNR aspect ratio, the pore diameter (5–200 nm) in the membrane template was adopted to control the width, while the amount of the deposited gold determines the length. Various templates have been used for synthesizing different anisotropic AuNPs: porous membranes [55], mesoporous silica [56], Si(100) wafers [55], pyrolytic graphite [57], polymers [58], nanoparticles [59], carbon nanotubes [60], inorganic clusters (e.g. $LiMo_3Se_3$) [61], surfactants organized in micelles [27, 47] as well as biomolecules (e.g. plant extracts) [62], microorganisms [63], polypeptides, and DNA [64].

3.2.3.5 Galvanic Replacement

Galvanic replacement is another approach for making anisotropic AuNPs. Without external current sources, Au cations in the plating bath are reduced by a metal in a spontaneously thermodynamically and kinetically favorable reaction [65]. The driving force of this reaction is the difference of the redox potential between the reducing metal and the Au^{3+}/Au^0 system. Intensively developed by Xia group, the reduction of Ag nanostructure has been used as a sacrificial template to fabricate hollow Au nanostructures [66, 67]. Starting from Ag nanocubes, anisotropic gold nanocages have been synthesized. These reactions proceed in two steps: formation of seamless hollow structures with the walls made of Au–Ag alloys by galvanic replacement; and subsequent formation of hollow structures with porous walls by dealloying [68]. In addition, aluminium is also used as the metal source since aluminium foil is inexpensive and has a very low oxidation potential which can reduce many transition-metal cations [69]. As fluoride forms stronger bonds than chloride, NaF and NH_4F were used to dissolve the alumina layer to allow the galvanic displacement, resulting in anisotropic Au dendrites [70]. The galvanic technique has some advantages such as no need of template, surfactant, or stabilizer, and can be conducted simply at room temperature, compared to the former methods.

3.2.4 Other Shapes of Anisotropic AuNPs

3.2.4.1 One-Dimensional (1D) AuNPs

Except for the widely investigated 1D anisotropic AuNRs, there are various remarkable shapes of anisotropic AuNPs. Among 1D structures, there are nanowires (NWs), nanotubes (NTs), and nanobelts (NBs). If the AuNRs continually grow to an extremely large aspect ratio, they become AuNWs, which generally show some mechanical flexibility. For example, the AuNRs stabilized by CTAB and pentahedrally twinned were used for preparing AuNWs by the tip-selective growth [71], generating crystalline AuNWs with 12–15 μm in length and 90 ± 10 nm in diameter. UV irradiation, photoreduction, and thermal reduction

were also used to make AuNWs [72]. With other metal elements such as Pt and Cu combining with Au, the bimetallic NWs can be fabricated [73]. Interestingly, the method of fabrication of AuCuNWs can also lead to the formation of AuCu nanotubes (AuCuNTs). Therefore, CuNWs were used as templates, and the AuCuNWs were formed as intermediates that ultimately led to the AuCuNTs [74].

Both AuNWs and AuNTs can be prepared by electroless deposition onto the pore walls of porous polymer membranes working as a template, and long Au deposition time leads to AuNWs while short time leads to AuNTs [75]. 4-(Dimethylamino)pyridine is a powerful auxiliary reagent for the electroless deposition method to yield AuNTs (Fig. 3.4) [76]. In other ways, hollow AuNTs with highly ordered Au arrays were synthesized by the galvanic replacement reaction using an anodized aluminum oxide template [77], a polymer NT as a sacrificial core [78], and thiol-functionalized nanoporous films as a scaffold [79].

Gold nanodumbbells (AuNDs) were synthesized by a modified seed-mediated method [80, 81]. The presence of tiny amounts of iodide stimulated tip growth prominently, resulting in well-defined dumbbell structures. Hybrid AuNDs were attractive according to their multiple functions. The Au/Ag core/shell structures have been created either by silver deposition onto AuNDs [82], or by galvanic replacement and reduction [83]. There are other metals for hybrid AuNDs, including CdSe [84], $CoPt_3$, FePt and Pt [85].

3.2.4.2 Two-Dimensional (2D) AuNPs

Beyond 1D structures, anisotropic AuNPs have 2D structures with well-defined specific shapes, such as stars, pentagons, squares/rectangles, dimpled plates, hexagons, and truncated triangles [86]. One widely used approach is using polymer templates, since the versatile polymers can act as stabilizers, templates, and

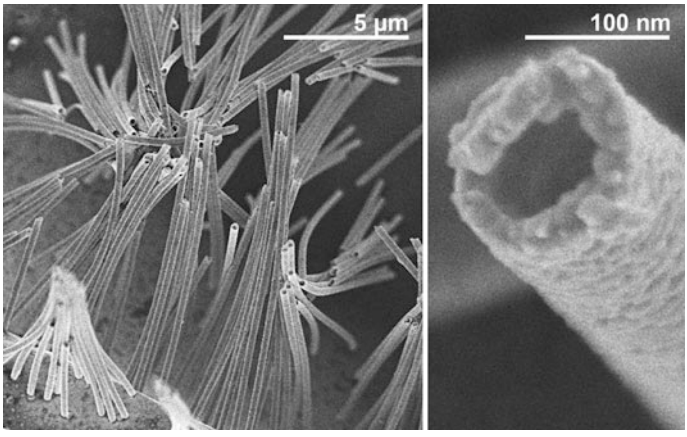

Fig. 3.4 SEM images of free-standing AuNTs [76]. Copyright 2010 American Chemical Society

reductants [72, 87–89]. For example, $PEO_{20}PPO_{70}PEO_{20}$ (PEO = poly(ethylene oxide), PPO = poly(propylene oxide)) was used as both the reductant and stabilizer to prepare large gold nanosheets (10 μm in width and 100 nm in thickness) [72].

The morphology could be finely adjusted through control of the reactant ratio and the reaction conditions. A large-scale synthesis of micrometer sized Au nanoplates was carried out [90]. Triangular and hexagonal gold nanoplates in aqueous solution were synthesized by thermal reduction of $HAuCl_4$ with trisodium citrate and CTAB, yielding gold nanoplates with the width as small as 10 nm to several hundreds of nanometers [91].

A mild and relatively environmental friendly one-pot biomimetic method was developed to fabricate gold nanoplates having hexagonal and truncated triangular structure with a thickness less than 30 nm [92]. The use of a biological reductant such as brown seaweed Sargassum [93], tannic acid [94], serum albumin protein [95], and glycine [96] was explored over the last decade. There is a type of special gold nanoplates having triangular nanoprisms morphology. These nanostructures show three congruent edge lengths in the range from 40 nm to 1 μm and a thickness ranging from 5 to 50 nm [97–99]. They can be prepared in high yields, which exhibit visible and IR LSPR.

3.2.4.3 Three-Dimensional (3D) AuNPs

For 3D anisotropic AuNPs, gold nanotadpoles have an interesting tadpole-like structure. They have special optical and electrical properties leading to unique potential applications in second-order nonlinear optics, nanoelectronics. Gold nanotadpoles were synthesized via a simple chemical procedure, i.e. in aqueous solution reducing chloroauric acid with trisodium citrate in the presence of sodium dodecylsulfonate as a capping agent, and the 3D crystalline structures were characterized by TEM, AFM, and HRTEM (Fig. 3.5) [100]. Tadpole-shaped AuNPs later were synthesized in high yield by a temperature-reducing seeding approach without any additional capping agent or surfactant [101]. The formation mechanism was ascribed to an aggregation-based growth process. A 3D hybrid nanostructure consisting of Au heads and Pd tails has been demonstrated, these 3D nanotadpoles were expected to display properties of both Pd nanorods and AuNPs [102].

Since branched gold nanostructures, such as monopods, bipods, tripods, tetrapods, hexapods, and multipods like nanoflowers, nanostars, and urchins have sharp edges and corresponding high localization of surface plasmon modes [103], they are anticipated for applications in nanocircuits and nanodevices, and in vivo tests, including biosensing [104], imaging [105], targeting [106], and photothermal therapy [107]. The branched AuNPs in aqueous solution was first synthesized by Carroll and co-workers in 2003 [108], using triangular Ag platelets as seeds and reducing Au^{3+} with ascorbic acid in the presence of CTAB leading to anisotropic Au monopods, bipods, tripods, and tetrapods. The dimension and number of branches were varied under combinations of the [seed]/[Au^{3+}] ratio in a seed-mediated synthesis approach [109]. There are other routes to produce branched

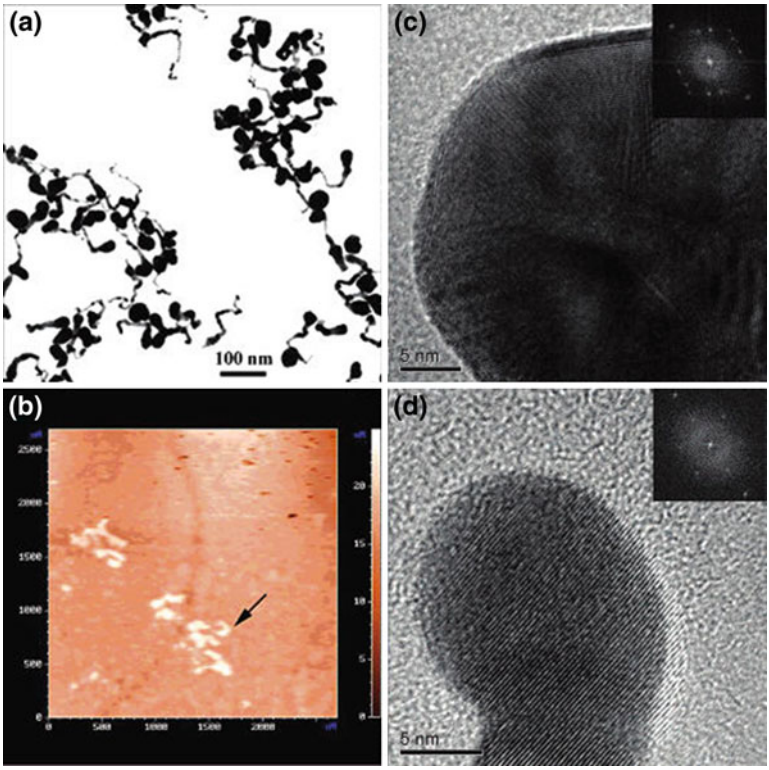

Fig. 3.5 **a** TEM and **b** AFM images of tadpole-shaped AuNPs. **c**, **d** HRTEM images of the **c** head and **d** tail of a gold nanotadpole. *Insets* The corresponding Fourier transform patterns [100]. Copyright 2004 American Chemical Society

AuNPs [110], with a high yield up to 90 % [111]. Generally, the branched AuNPs have poorer monodispersity than other shapes.

For the branched nanoparticles, they have complicated LSPR consisted of multiple sharp peaks in the visible and NIR region. The study showed the resulting LSPR energies can be considered as a hybridization of the core and tip plasmons (Fig. 3.6) [112].

Interestingly, another type of anisotropic AuNP dendrites exhibits the hierarchical tree-type architecture with trunks, branches, and leaf components. With such hyperbranched architectures, they have attracted much attention for their fascinating fractal growth phenomena and their potential applications in functional devices, plasmonics, biosensing, and catalysis [113, 114]. They are mainly synthesized by electrochemical deposition. For example, Au dendrites are synthesized on a glassy carbon electrode by electrodeposition with a square-wave potential from a solution of $HAuCl_4$ containing cysteine as the blocking molecule [113]. Shape-controlled synthesis of Au dendrites was achieved in the presence of supramolecular

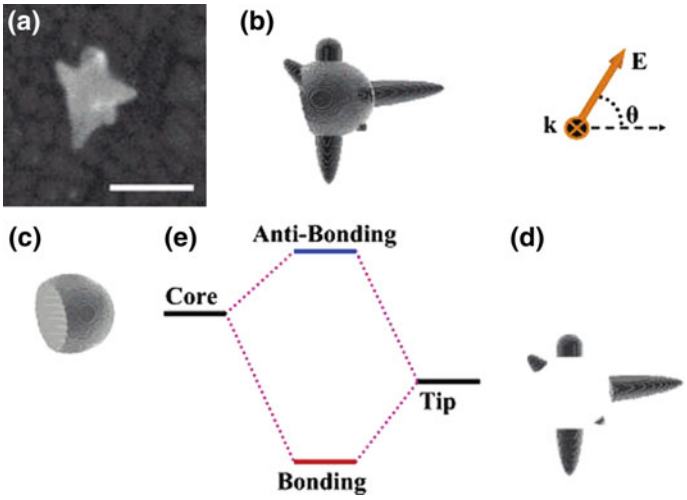

Fig. 3.6 Principle of the plasmon hybridization of the LSPR of a gold nanostar. Panel **a** shows an experimental scanning electron micrograph. The scale bar is 100 nm. Panel **b** shows the theoretical model, consisting of a truncated spherical core, (**c**) and tips, consisting of truncated prolate spheroids (**d**). Panel **e** illustrates the concept of plasmon hybridization in the nanostar. The core plasmons interact with the tip plasmons and form bonding and antibonding nanostar plasmons. The polarization angle is defined in the *upper right corner* [112]. Copyright 2007 American Chemical Society

complexes formed from dodecyltrimethylammonium bromide (DTAB) and *β*-cyclodextrin (*β*-CD) (Fig. 3.7) [115].

A typical core/shell nanostructure contains a supporting core and a thin Au nanoshell, for example, SiO_2@Au NPs exhibit a strong plasmon resonance, and core radius and shell thickness dependent SERS effect [116]. The plasmon wavelength could be tuned by varying the relative size of the inner and outer shell layer over a wide range from visible to IR spectrum, of which the NIR region between 700–1100 nm is particularly useful in biomedical applications, such as therapy and diagnostics [117]. There are other metal or metal oxide cores used to replace SiO_2 [118]. For example, Fe_3O_4@Au core/shell NPs modified with antibodies and fluorescent dyes work as contrast probes for the multimodal imaging of tumors [119]. In a more complicated system, covering a magnetic Co@Au core/shell NPs with a pure Co core and an intermediate Au shell, a compact outer cobalt oxide shell was further coated on it [120].

A layer of hard inorganic nanomaterials is used for surface modification of AuNRs, showing advantages of increasing stability, facilitating surface chemistry, and tunable properties. Silver coating on AuNRs is successfully accomplished whose thickness can be controlled through the concentration of silver precursors and reducing agents [121]. The silver coated AuNRs have practical application in enhancing Raman scattering [122]. Silicon coatings can be achieved by simple addition of aqueous sodium silicate to the AuNR solution, which is then mixed with

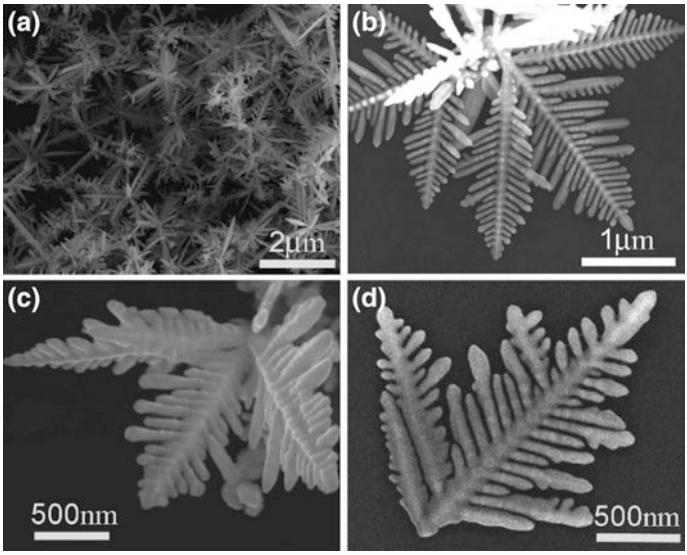

Fig. 3.7 SEM images of Au nanodentrites grown in mixed DTAB/β-CD solution, [DTAB] = 5.0 mM; [β-CD]/[DTAB] = 0.5. From [115]. Copyright 2009 American Chemical Society

3-mercaptopropyl trimethoxysilane (MPTMS) or 3-mercaptopropyl triethoxysilane (MPTES) solution, forming mesoporous silicon shell on AuNR surface resulting in red-shifted longitudinal LSPR [123]. Other hard inorganic coating layers on AuNRs have been explored such as iron oxide coating [124], platinum coating [125], and silver sulfide or selenide [126]. These inorganic layers coated AuNRs have promising applications of magnetic separation, imaging, catalysis, and optical nonlinearities.

Hollow gold nanospheres (HAuNSs) were synthesized by layer-by-layer (LbL) assembly [52, 127]. Through the size-controllable LbL technique, HAuNSs were deposited on a sacrificial template of polyelectrolyte-modified polystyrene (PS) nanospheres. Afterwards, the PS core was removed by either calcination or dissolution [128].

Recently, there is a novel class of remarkable nanostructures gold nanocages (AuNCs) possessing hollow interiors and porous walls synthesized by galvanic replacement [129], which have potential in colorimetric sensing and biomedical applications. During synthesis, $HAuCl_4$ solution was added to a boiling suspension of Ag nanocubes which act as both template and reducing agent in a controlled manner. Due to the difference of electrochemical potential between Au and Ag (the reduction potential of $AuCl^{4-}$/Au: 0.99 V, of AgCl/Ag: 0.22 V versus the standard hydrogen electrode), there happened galvanic replacement and thereby Au deposited on Ag nanocube surface. The resulting hollow, porous cage-like Au nanostructures were characterized by SEM and TEM [129]. For a representative process

and structure (Fig. 3.8), nanoboxes derived from 50 nm Ag nanocubes were first converted into nanocages. Then by increasing the amount of the etchant $Fe(NO_3)_3$ during the dealloying process, only porous cubic nanoframes were left [130].

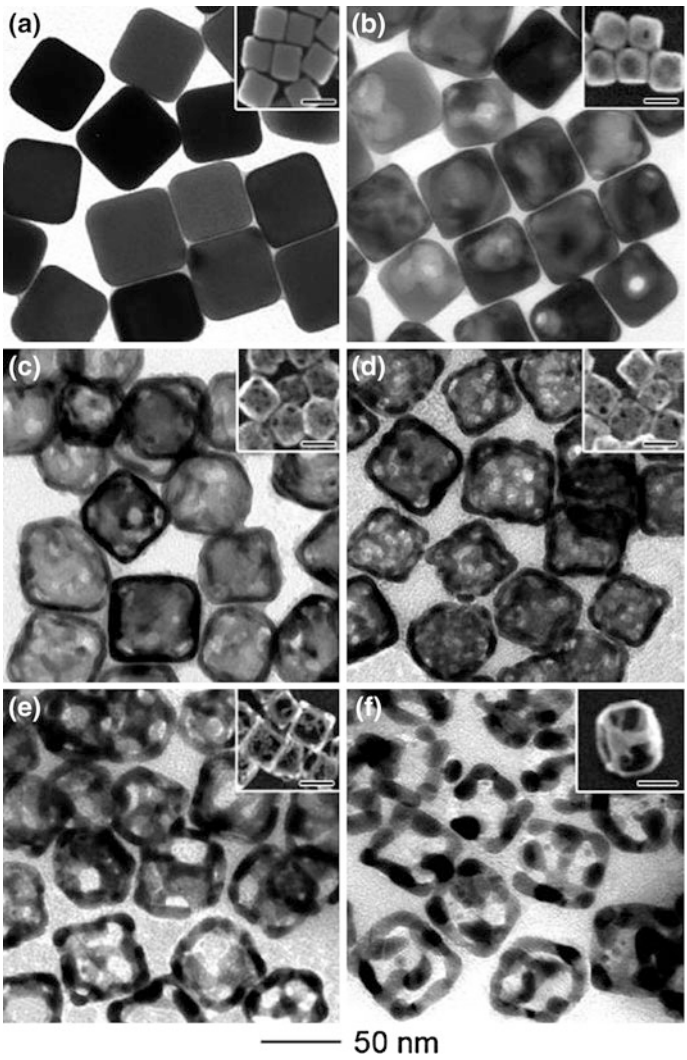

Fig. 3.8 TEM and SEM (*inset*) images of **a** 50-nm Ag nanocubes; **b** Au/Ag alloy nanoboxes obtained by reacting the nanocubes with 4.0 mL of 0.2 mM $HAuCl_4$ aqueous solution; and **c**–**f** nanocages and nanoframes obtained by etching the nanoboxes with 5, 10, 15, and 20 μL of 50 mM aqueous $Fe(NO_3)_3$ solution. The inset in (**f**) was obtained at a tilting angle of 45°, clearly showing the 3D structure of a nanoframe. The scale bars in all insets are 50 nm. EDX analysis indicates the atomic ratio of Au:Ag was 15:85, 30:70, 45:55, 60:40, and 100:0 for the samples in panels b, c, d, e, and f, respectively [130]. Copyright 2007 American Chemical Society

3.3 Properties

3.3.1 Morphology

For the AuNPs synthesized by seed-mediated growth approach [109], AuNPs generally show morphologies of tetrahedron (four triangles) [131], hexahedron (cube, six squares) [132], octahedron (eight triangles) [133], dodecahedron (twelve pentagons) [134], and icosahedron (twenty triangles) [135], which are characterized by low-index facets ({111} for tetrahedron, octahedron, dodecahedron and icosahedron, and {100} for the cube. AuNPs also showed rhombic dodecahedral shape [133], which could further transform into other nonplatonic shapes such as rhombic cuboctahedron and then truncated octahedron in the presence of PVP at a low water content [109].

3.3.2 Optical and Photothermal Property

One characteristic property of AuNPs is that they exhibit LSPR, an optical phenomenon leading to confined resonant photon within the dimensions of the AuNPs when a AuNP interacts with incident photons, which results in an oscillation of the conduction band electrons back and forth on its surface and further induces a charge separation between the free electrons and the ionic metal core, and thereby generates a dipole oscillation [136]. The LSPR oscillation of the colloidal AuNPs usually results in a certain color of the solution that has a strong absorption signal in the visible region. The LSPR is dependent on the particle material, size, shape and the dielectric properties of the surrounding medium [137]. For spherical AuNPs, both light absorption and scattering are enhanced by AuNPs, which cause light extinction [138]. Based on Mie theory and relative Gan theory [139], quantitative description of the cross-sections of absorption (C_{abs}), scattering (C_{sca}), and total extinction (C_{ext}) are derived [140].

Different from those of spherical AuNPs, anisotropic AuNPs have their own particular LSPR. Normally, AuNPs with core diameters between ~3 and 200 nm display a LSPR with a maxima intensity at approximately 520 nm. AuNRs are well known for their characteristic LSPR signals: once the symmetry of the gold core is altered to the anisotropic AuNRs, two distinct LSPR modes corresponding to the different axes across the AuNRs emerged, i.e. a transverse LSPR along the short axis and a longitudinal LSPR along the long axis. Typically, the longitudinal LSPR peak will red shift when the aspect ratio increases, which has been investigated by simulation and demonstrated in experiments [138]. A representative experimental example is displayed in Fig. 3.9 [141]. Quantitatively, it has been discovered that there is a linear relationship between the peak position and aspect ratio [47]:

$$\lambda_{max} = 95R + 420$$

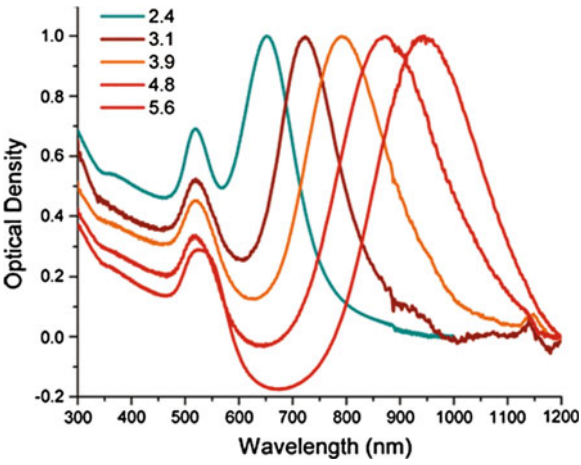

Fig. 3.9 Surface plasmon absorption spectra of AuNRs of different aspect ratios, showing the sensitivity of the strong longitudinal band to the aspect ratios of the AuNRs [141]. Copyright 2006 American Chemical Society

Owing to the interesting photothermal effect of AuNRs, they show promising biological and biomedical applications. When AuNRs are exposed to the laser light resonant with their surface plasmon oscillation, they can strongly absorb the light and rapidly convert it into heat via a series of photophysical processes. The mechanism was investigated and explained by El-Sayed group [142]. When the heating rate is much faster than the cooling rate, heat is accumulated within the lattice causing a temperature rise of the AuNRs in a short time which is sufficient enough to lead to structural changes, such as shape transformation and particle fragmentation. For example, when a colloidal AuNR solution was exposed to femtosecond laser pulses (100 fs, 52 μJ) [143], the shape transformation is observed as shown in Fig. 3.10. The wavelength of the exciting laser (800 nm) coincides with longitudinal plasmon absorption of AuNRs. In Fig. 3.10b, all the AuNRs have transformed into spheres. For the UV-vis spectrum in Fig. 3.10c, only one LSPR band at about 520 nm exists for typical spherical AuNPs and the longitudinal plasmon band has totally disappeared. In Fig. 3.10d, the volume of the resulting spherical particles is similar to the original AuNRs, which concludes that AuNRs melt into spherical AuNPs under the intense laser irradiation based on photothermal effect. From more exploration, it was discovered that the shape transformation of AuNRs depends on laser's energy and pulse-width [143], and the unusual photothermal melting process and its mechanism were investigated [144]. Also there are other related spectral properties such as the aspect ratio dependent fluorescence [145], shape-dependent electron-photon relaxation [146] and LSPR line width (for sensing local environmental changes for biomolecular recognition) [147].

Since AuNRs have important applications in sensing, plasmon-enhanced spectroscopies, biomedical imaging, and photothermal therapy for cancer, controlling the shapes (aspect ratio) and sizes of AuNRs with desired physical and chemical properties are required, which are crucial for their performances [148]. For example, AuNRs with larger aspect ratio have response to NIR light and therefore are

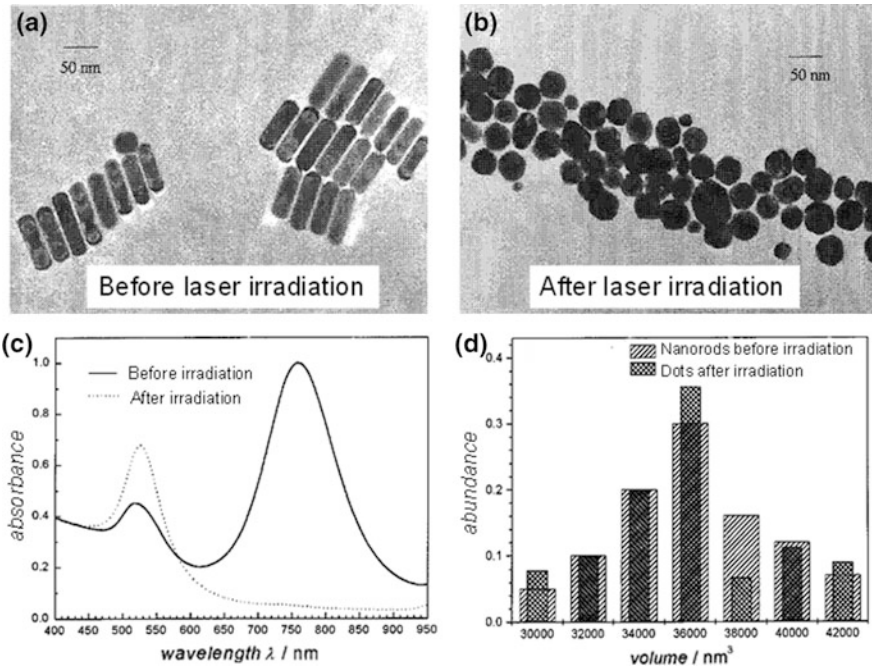

Fig. 3.10 Effect of laser heating on AuNRs, shown in TEM images of a colloidal AuNR solution having a mean aspect ratio 3.8 before (**a**) and after (**b**) irradiation with 100 fs laser pulses centered at 800 nm. **c** UV-vis absorption spectra of this colloidal gold solution before (*solid line*) and after (*dotted line*) irradiation with laser pulses. **d** The volume of the AuNRs before and after this laser irradiation is compared [143]. Copyright 1999 American Chemical Society

excellent candidates for photothermal therapy. At a fixed aspect ratio, larger AuNRs having larger extinction coefficients due to stronger light scattering provide better performance in optical imaging applications, whereas smaller AuNRs provide improved efficiency in photothermal therapy applications due to their higher absorption efficiency [149]. The plasmon bands of other anisotropic AuNPs with different shapes have been also explored [129, 150]. Typically, there are bands from separate parts and ensemble structure. For example, gold nanostars show a plasmon band of the core and variant plasmon bands relating to the tips and core–tip interactions [111].

3.3.3 Surface Enhanced Raman Scattering (SERS)

Because of the plasmon resonance, the Raman signals depending on the power of the local electric field is very high at the AuNP surface. Originating from the dramatic amplification of electromagnetic fields in the AuNP ensembles, AuNPs in

close proximity to each other will result in near-field interparticle interactions, creating a collective extinction response that is quite different from the individual ones [151]. Excitation of the LSPR produces a strong electromagnetic field at the surface of the AuNP that can interact with materials in close proximity to the AuNP surface [22, 152]. The plasmon electromagnetic field can therefore be used to enhance the scattering spectra of chemical species adsorbed on AuNPs, a phenomenon known as surface enhanced Raman scattering (SERS) or to detect changes of specific analytes in the local chemical environment. For anisotropic AuNPs, the Raman scattering signal of molecules is enormously enhanced by contributions from the strong absorptions in the NIR regime and the extremely high electric field intensities at the tip or hollow structures [153]. Therefore, it is necessary to control the size, shape, and structure of anisotropic AuNPs to effectively enhance the sensitivity of effective molecular detection [77, 154]. The most attractive ones are AuNRs because of their easily accessible anisotropic shape and tunable size. There are two coupling fashions for AuNRs: side-by-side and head-to-head configurations which result in different shifts of LSPR signals: the one with side-by-side geometry shows a blue-shift in the longitudinal LSPR and a red-shift in the transverse LSPR, while the other with head-to-head geometry shows a red-shift in the longitudinal LSPR with little change in the transverse LSPR [155]. Such plasmonic coupling effect is an emerging field which is of great interest to SERS applications for molecular detecting as the SERS effect of AuNRs is much higher (e.g. 10^5 times) than spherical AuNPs [156]. On the aspect of biomedicine, AuNRs aligned by oral cancer cells showed excellent sensitivity in detecting the cancer cells [157]. Acidic cancer cells and healthy cells are distinguished by monitoring changes in the Raman spectrum induced by pH changes of carboxy groups in a mercaptobenzoic acid layer on HAuNSs which have activity in NIR region [158].

3.3.4 Fluorescence Enhancement and Quenching

The interaction between AuNPs and a fluorophore results from a change in the electromagnetic field and the intensity of the photonic mode near the fluorophore. For AuNP–fluorophore distances less than 4 nm, the fluorescence is strongly quenched. At larger distances, the fluorescence intensity is increased. For fluorescence quenching, characteristic fluorescence of organic dyes such as perylene and porphyrin attaching on AuNP and AuNR surface via Au–S linkage with distance less than 4 nm were significantly quenched (Fig. 3.11) [159, 160]. In another experiment, the simple inert short *n*-C_{10} alkyl chain protected AuNPs with different size and AuNRs could quench the perylene diimide dyes (PDIs) close to their surface, from which the mechanism of such quenching effect was investigated and ascribed to energy transfer [161]. The fluorescence enhancement originates coupling with far-field scattering. For example, the quantum yield of indocyanine green (ICG), a NIR fluorophore, was increased by up to 80 % near the surface of an Au

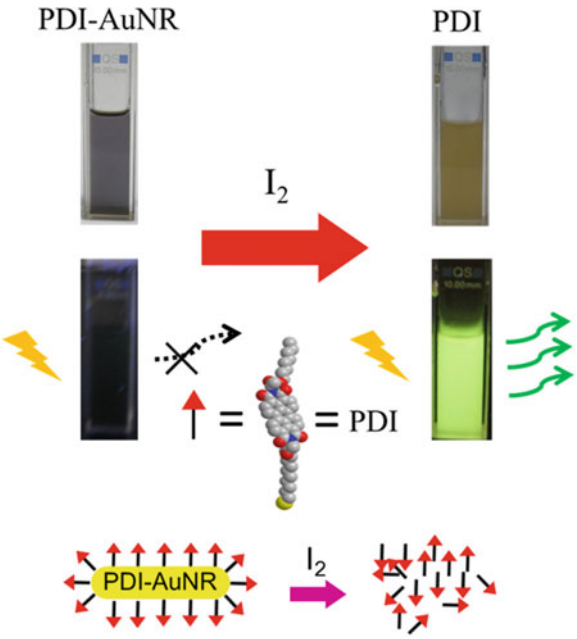

Fig. 3.11 *Left* PDI-AuNR CH_2Cl_2 solution shows no emission under UV lamp (365 nm, 6 W). *Right* free PDI after detaching from PDI-AuNR by adding I_2 in CH_2Cl_2 solution shows strong *yellow −green* fluorescence under UV lamp [160]. Copyright 2012 American Chemical Society

nanoshell. Such conjugates have been used for enhancing sensitivities in fluorescence imaging in vitro and in vivo [162].

3.3.5 Toxicology

In general from in vitro studies, AuNP cores are nontoxic for cells, which are in contrast with other nanoparticles such as carbon nanotubes, asbestos, and metal oxides causing drastic damage to cells. Anisotropic AuNPs have an enormous potential in theranostics and addressing the in vivo nontoxicity of these AuNPs are essential to convince drug administration. In vitro and in vivo toxicology studies have been undertaken to examine the damage of cells, tissues, and organs of animals upon loading AuNPs for biomedical applications [22, 163].

In vitro studies have shown that the toxicity of AuNRs is ascribed to the CTAB ligands, rather than the Au core itself. Researchers successfully found biocompatible materials such as polyacrylic acid or poly(allylamine) hydrochloride to coat AuNPs, resulting in almost no death of cells [164]. For citrate-capped AuNPs, a study in mice by Chen et al. showed that small (3–5 nm) and large AuNPs (30 and 100 nm) were not toxic, but medium-sized AuNPs (8, 12, 17, and 37 nm) provoked severe sickness, loss of weight, change in fur color, and shorter life spans due to injury of the liver, spleen and lungs [165].

For the stability issue of AuNPs in biosystems, it is also an important subject to be investigated, since AgNPs are as intrinsically toxic for their relative easy

oxidation to Ag^+. On contrary, Au^0 is much more difficult to oxidize than Ag^0, which guarantees the safety issue of AuNPs. The AuNP cores of isotropic AuNPs larger than 5 nm are biologically inert [22, 166]. However, for the anisotropic AuNPs with highly exposed AuNP surface areas and defects, more studies are required aiming at the toxicology in biosystems.

3.3.6 Surface Modification

Surface modification not only provides stability to the AuNPs, but also introduces foreign functions. In addition, to introduce AuNPs into biosystems, it requires surface modification for desirable compatibility with the systems.

A number of organic materials are used to functionalize AuNPs and introduce multiple functions. This has been realized by the exchanging process in which the surface grafted surfactant molecules exchange with functional organic molecules, usually a type of organic thiols (RSH) or a mixture of two kinds of organic thiols. Owing to the strong covalent Au–S bondings, this is a relatively simple and effective procedure that can completely remove the original surfactants and replace with organic functional thiols on the entire surface. For the organic thiol monolayer protected anisotropic AuNRs, the solubility, surface chemistry and related properties are dominated by the organic shell. Simple *n*-alkyl thiols [167], and other functional materials such as photoresponsive azo thiols [168], chiral-azo thiols [169], organic dyes (porphyrin, perylene) [159, 160] and polymers terminated with thiols (poly2-(dimethylamino)ethyl methacrylate, poly(acrylic acid), polystyrene) have been used [170].

Different from isotropic AuNPs, AuNRs have unique properties in thiol exchange process and the resulting AuNRs have more shape-dependent properties. For example, the seed-mediated growth approach prepared AuNRs coated by CTAB with open positions on the two heads where there are no CTAB surfactant molecules covering [29]. Therefore, the thiols will first bind on the open tips of these AuNRs and then replace the CTAB surfactants on sides, leading to sequential surface modification of AuNRs which induce more functions such as directed self-assemblies, including side-by-side and head-to-head types [171].

Another effective way to functionalize the surface of AuNR is covering the surfactant layer (e.g. CTAB) with materials having intermolecular interactions such as electrostatic and ionic interaction to CTAB molecules. With the presence of the CTAB layer on the surface imparting a net positive charge, alternate adsorption of anionic and cationic polyelectrolytes on these positively charged AuNRs leads to the formation of polyelectrolyte multilayers around the AuNRs [172, 173]. One representative example of AuNRs coated by polyelectrolytes multilayers [poly acrylic acid sodium salt (PAA) and polyallylamine hydrochloride (PAH)] is displayed in Fig. 3.12, which briefly indicates the process of layer-by-layer coating on AuNRs and encapsulating of functional small Rhodamine 6G molecules.

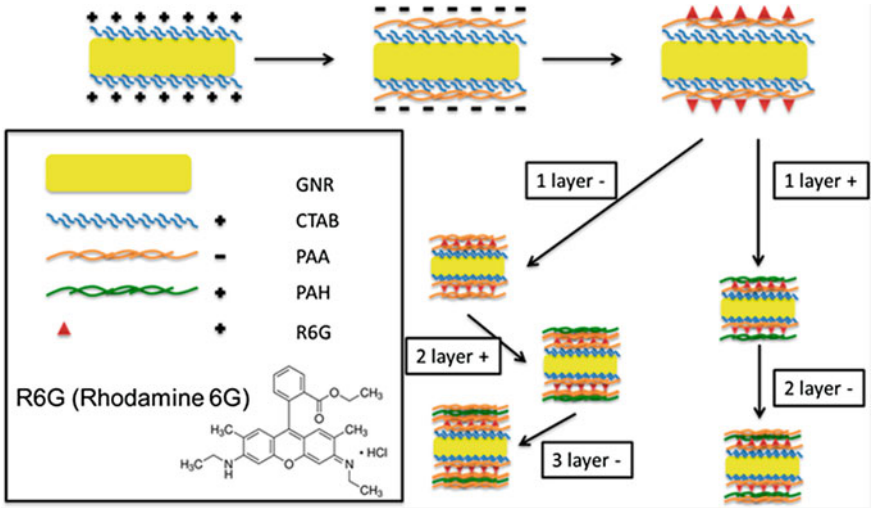

Fig. 3.12 AuNR coated with layer-by-layer polyelectrolytes where and R6G is wrapped in different types of polymer layers [173]. Copyright 2012 American Chemical Society

The critical prerequisite to introduce AuNRs into the biosystem is to functionalize AuNRs with biocompatible materials, because for potential clinical trials, AuNRs should be friendly to human health and the environment. With the widely used seed-mediated synthesis approach, AuNRs are coated by a CTAB layer. Free CTAB molecules are detrimental to human cells but surface bound CTAB molecules are not toxic [174] and AuNRs are supposed to be safe for in vivo and clinical studies. However, although free CTAB molecules can be separated by centrifugation or dialysis membrane, CTAB surfactants could leave AuNR surface because they are dynamically unstable. The charge interactions that adsorb CTAB on AuNR surface are much weaker than Au–S covalent bonds. Therefore, a better way is to modify the AuNR surface that CTAB is either replaced or covered by biocompatible molecules. For example, by coating phosphatidylcholine on AuNRs, there was much lower cytotoxicity than the twice-centrifuged CTAB-AuNRs [175]. Poly (diallyldimethylammonium chloride)-AuNR, poly(4-styrenesulfonic acid)-AuNR even showed no observable toxicity [176]. Another simple approach to prepare biocompatible AuNRs is using polyethylene glycol polymers (PEG), via mixing PEG-SH with the CTAB-AuNR in solution undergoing thiol exchange for hours [177]. More experiments have been carried out to conjugate biomolecules to AuNRs and mainly four different methodologies have been developed: (a) direct ligand exchange, (b) electrostatic adsorption, (c) the use of a biofunctional linker, and (d) surface coating [148].

The thiol exchange reaction is effective for small biofunctional molecules such as 3-mercaptopropionic acid (MPA) [178], but challenging for large molecules such as antibodies and proteins that are too large to reach the AuNR surface because of the densely packed CTAB layer.

3.3.7 Supramolecular Organizations (Self-assembly and Alignment)

The functional molecules providing attractive intermolecular interactions on the surface of AuNPs could work as molecular "glue" to assist anisotropic AuNP assemblies. For anisotropic AuNPs, the LSPR allows them to concentrate and manipulate light depending on their size, shape and proximity and assemblies in specific patterns. For example, AuNRs having head-to-head or side-by-side assembly fashions exhibit distinct collective properties due to plasmon coupling between them, which are different from those of both individual AuNRs and bulk materials [109, 179]. Controlling and tuning anisotropic AuNP self-assemblies are highly interesting and vital. The AuNR self-assembly might potentially contribute to the preparation of metamaterials with unusual electromagnetic properties [180]. To achieve AuNR self-assemblies, intermolecular interactions offered by functional materials on AuNR surface can be exploited. So far, promising AuNR self-assembly nanostructures have been developed. Bifunctional small molecules with a thiol on one end for binding onto AuNRs and another functional group on the other end providing intermolecular interaction are used to promote head-to-head AuNR assemblies. The first chemically driven assembly of AuNRs by DNA was reported by Dujardin et al. who assembled AuNRs in parallel stacks by DNA hybridization [181]. Appropriate choice of the thiolate ligands (e.g. 1,2-dipalmitoyl-sn-glycero-3-phophothioethanol) [182] or mercaptopropylsilane [183]) and solvent evaporation are joint to prepare side-by-side assembly of AuNRs. Recently, prominent results have been found. For example, with hydrophobic favoring effect, AuNRs with PS on AuNR tips resulted in impressive linear chain like head-to-head assemblies (Fig. 3.13) [171]. Functional groups, providing streptavidin bridging, hydrogen bonds and DNA hybridizations, are good candidates. For example, AuNRs are functionalized with thioacetic acid at the ends and further conjugated to anti-mouse IgG [184]. Mouse IgG having two binding sites with the AuNRs is added and initiated AuNR head-to-head assemblies forming linear chains up to 3 mm.

Apart from thiols, Pan et al. [185] showed that the AuNRs can be directly assembled into 1D and 2D architectures via the electrostatic interaction between DNA and AuNRs. Such assemblies via ionic interaction were also demonstrated using adipic acid [186], citrate molecules [187], and dimercaptosuccinic acid [182]. By using Gemini surfactants replacing CTAB during AuNR growth, the resulting AuNRs can self-assemble even into standing superlattices formed during drying [188]. This method has also been applied to inorganic Ag layer coated AuNRs, which form similar 3D super lattices of AuNR side-by-side assemblies, demonstrating highly efficient SERS [189].

Furthermore, inducing AuNR alignment in thin film is of particular importance for their practical applications [190, 191]. In early work, an electric field was tested to induce AuNR alignments in solution [192]. Recently, Lavrentovich group has applied electric field to align colloidal AuNRs in a concentric fashion to

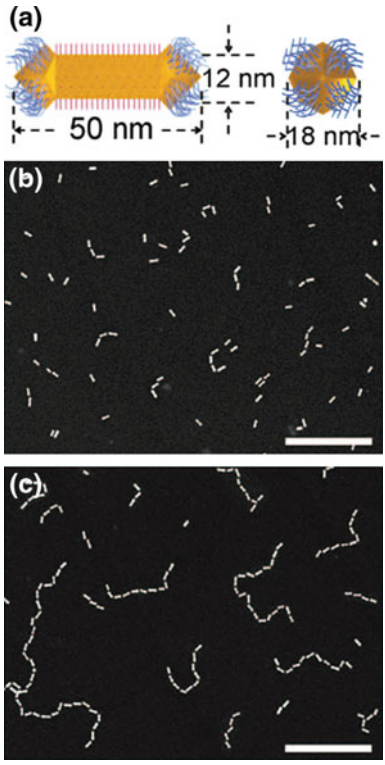

Fig. 3.13 **a** Schematics of the side view of the long face (*left*) and the edge (*right*) of the AuNR carrying CTAB on the long side and thiol-terminated PS molecules on the ends. (**b** and **c**) Darkfield TEM images of the AuNR chains after 2 (**b**) and 24 (**c**) hours assembly. $[M]_0 = 0.84 \times 10^{-9}$ (mol/L). Scale bar, 100 nm (both panels) [171]. Copyright Science 2010

demonstrate cloaking effect, which is similar to the simulated prediction model [193]. LCs provide a long range orientational order to assist AuNR alignments which also respond to external field such as mechanical, electric and magnetic field. Lyotropic LC hosts that form nematic and hexagonal phases can be quite advantageous in aligning a high loading of AuNRs which are functionalized with micelles on surface [194]. Recently, organo-soluble thermotropic LCs were also used for such purpose [195]. In solid medium, polymer engineering is an attractive strategy to assemble AuNRs. AuNRs dispersed poly(2-vinyl pyridine) (P2VP) polymer films exhibit controllable optical properties through AuNR self-assembly and percolations [196]. There are other polymers such as poly(*N*-isopropylacrylamide) and its acrylic acid derivative [197, 198], poly(vinyl alcohol) (PVA) [191, 199], poly (styrene-b-methylacrylate) [200] enable fabrication of anisotropic arrangements of AuNPs. For example, colloid AuNRs were embedded during the polymer preparation. The alignment of AuNRs can be confirmed by polarized light: with the electric field of the incident light parallel or perpendicular to the alignment direction of AuNR, only the longitudinal or the transverse LSPR band can be excited and detected [191]. In another way using patterned channels, translational ordered AuNR arrangements have been fabricated by the synergetic self- and directed-assembly processes and lithography [201].

3.4 Applications

Unlike spherical AuNPs, there are more remarkable plasmonic phenomena of anisotropic AuNPs. Among them, particularly for AuNRs with exceptional optical properties, a variety of applications have emerged including biological and biomedical applications such as biosensing, biomedical imaging, gene and drug delivery, disease detection, diagnosis, plasmon-enhanced spectroscopy, and photothermal cancer therapies [22, 142, 202].

3.4.1 Catalytic Application

The catalytic activity and sensitivity of metal NPs (MNPs) are dependent primarily on their size and shape. As a consequence of the presence of sharp edges and corners, the number of active surface sites in anisotropic AuNPs is very high compared to spherical AuNPs. Therefore nano-engineering is crucial in tailoring NP properties.

A breakthrough in catalysis research that opened up a wide area of AuNP-catalyzed oxidation reactions [203] is carbon monoxide (CO) oxidation by dioxygen at low temperature catalyzed by small (<5 nm) AuNPs on titanium oxide [204]. It is widely accepted that CO molecules are preferentially adsorbed at edges and steps on the surface of AuNPs rather than on the facets. For example, it was shown that the perimeter interfaces around AuNPs are the sites for CO oxidation [205]. Thus, research interests in such catalysts began to focus on anisotropic AuNPs [206], which show higher catalytic efficiency than simple AuNPs due to more edges and steps on anisotropic ones [207]. Some hybrid bimetallic anisotropic AuNPs also exhibit high activities in various catalytic reactions [208–210], e.g. for the tandem reaction of alcohols and nitrobenzenes to generate N-alkyl amines and imines [209].

3.4.2 Sensors and Molecular Recognition

Since the strong affinity between anisotropic AuNPs and heavy metal cations can alter the position of the plasmon band of AuNRs or the fluorescence of targeted ions, it allows detecting heavy metal cations in aqueous solutions with ultrahigh sensitivity without sample pretreatment. Since the LSPR frequency of AuNRs depends on the dielectric constant of the surrounding medium, the shift of LSPR band provides an opportunity to monitor the changes of the local environment, which can be used for sensors [211]. There are many examples of functionalized AuNRs for devices including multiplex colorimetric detection [212, 213]. Heavy metal ions are widely distributed in biological systems that play an important role in

many biological and environmental processes. The analytical determination of toxic metals is an important issue in both environmental monitoring and clinical research [214]. Currently, AuNRs are the most widely used anisotropic AuNPs for detecting heavy metal ions. A multiplex biosensor assay using different responses of AuNRs relating to different targets is developed [215], in which human, rabbit, and mouse immunoglobulin G (IgG) were conjugated to AuNRs with different aspect ratios via a MUDA linker. Variant shifts of the LSPR wavelength of AuNRs were monitored when binding to their respective complements (anti-IgGs). Except for the absorption spectrum shift of AuNRs, the scattering wavelength shift from individual AuNRs was also reported in biomolecular protein sensing [213]. Single molecular DNA detection is achievable by using AuNR sensors linked to F1-ATPase motors in dark field microscopy [216].

In recent years, AuNRs as SERS probes in biological applications were intensively investigated [156, 217]. The reasons are: they have strong SERS enhancement; their LSPR bands can be tuned by the aspect ratio to match with the excitation laser (especially in the harmless red to NIR region); and they have proper size (length scale of 20–100 nm) with optimal enhancement [217]. Although using SERS effect for sensing was first discovered based on spherical AuNPs [218], AuNRs show much stronger SERS enhancement with the factors on the order of 10^4–10^5 due to the lightening-rod effect [156]. One representative example is peptide-conjugated AuNRs for molecular cancer diagnosis [219].

The AuNRs with various functionalized ligands on the surface exhibit the variation in the characteristic longitudinal plasmon absorption when in contact (coordination) with metal ions. Cysteine (Cys) modified AuNRs have been used as colorimetric probes in the titration of Cu^{2+} ions. The strong coordination of Cu^{2+} ions with cysteine results in a stable Cys-Cu-Cys complex and induces the aggregation of the AuNRs along with a rapid color change from blue-green to dark gray [214]. Dithiothreitol (DTT) modified AuNRs were used as a LSPR sensor of Hg^{2+} ions. In this case, the DTT molecules were strongly adsorbed on the surface of the AuNRs through thiol groups and induced the aggregation of AuNRs. The induced aggregation of AuNRs was inhibited in the presence of Hg^{2+} ions, and the aggregation level was dependent on the concentration of Hg^{2+} ions. The degree of aggregation could be determined by the change in the intensity of the longitudinal plasmon absorption in the UV/Vis spectrum [220]. The detection of some other metals such as Cr^{6+} and Pb^{2+} was recently reported by using a similar method [221].

Besides the change of longitudinal plasmon absorption signal, fluorescence is another effective method for ion detection, for example for the detection of Hg^{2+} ions in a homogeneous medium, with AuNRs used as a fluorescence quencher [222]. Nanowires are required for applications such as ultrasensitive and multiplex DNA detection through SERS and other biomedical SERS-based techniques [223]. Bimetallic AuPtNWs are useful electrochemical sensors for glucose with increased selectivity, sensibility, and repeatability compared to monometallic nanowires [73].

Besides AuNRs, other shapes of anisotropic AuNPs also have advantages for biosensors [224]. Au nanopyramids, nanotubes, nanocages, nanowires, nanostars and Au@Ag NRs have been reported as biosensors and bioprobes [225]. These

anisotropic AuNPs functionalized with specific molecules (small molecules, DNA, antibodies, and biotin) can recognize particular nano-objects (protein, DNA, drugs, and streptavidin) based on the change in the plasmon absorption, or the SERS intensity. Conical AuNT/pores can be advantageous to avoid unwanted plugging and are ideally suited to detect protein-type bioanalytes [226]. Au nanoplates exhibit a wide range of unique electrical and optical properties. For example, they show significant SERS [227], tip-enhanced Raman scattering (TERS) [228], and a shape- and size-dependent surface plasmon absorbance in the visible to IR region, which have potential applications in sensors and probes [228]. Dendritic AuNPs exhibited significant catalytic activities, and the good SERS sensitivity for the detection of biomolecules also indicated their potential applications in biosensing and nanodevices. SiO_2@Au NPs were applied to optical imaging [229], biomedical detection [230], and photothermal cancer therapeutic ability [231], and may enable a new class of infrared materials, components, and devices to be developed. AuNCs and Au nanoframes were investigated in catalysis [232] and biosensing in view of their controllable LSPR properties that depend on the size and, most importantly, the thickness of the walls [233].

Similar to biosensors described above, with the same principle of showing LSPR shifts, anisotropic AuNPs are used for molecular recognition. For example, functionalized AuNRs and Au nanoplates have been used for organic solvent recognition, toxin recognition and glucose recognition, respectively [94, 234, 235].

3.4.3 Nanoelectrodes

Anisotropic AuNPs have also been used in electrochemistry applications. Au nanotubes were applied as nanoelectrodes showing a much higher sensitivity (more than twice) than the embedded Au nanoelectrodes, which could be used in applications like molecular detection [236]. The AuNWs and AuNTs synthesized in this way can be used as nanoelectrodes, molecular filters, and chemical switches [75].

3.4.4 Biomedical Applications: Imaging, Diagnostics and Therapy

3.4.4.1 Imaging

AuNRs, HAuNSs, AuNCs, and Au nanostars are remarkable anisotropic AuNPs for biomedical applications because: (1) they have a large absorption in the NIR window for photothermal therapy; (2) they can selectively accumulate at sites of interest through the enhanced permeability and retention (EPR) effect or by surface modification with specific coatings; (3) their simple functionalization (e.g. with PEG) and structural features allow their use as nanocarriers for drugs, DNA, or

RNA; and (4) they have long body circulation times [129, 237]. The emerged term "theranostic" of AuNP nanocomposites combines functionalities of both contrast agent and therapeutic actuators within a single nanoparticle. Au nanoshells were the first AuNPs to be used as efficient theranostic agents that combine imaging and phototherapy functions [162].

The development of new techniques to diagnose cancer early is contributing to increase the cancer survival rate. To detect the cancer cells, AuNPs such as spherical Au nanoshells [162], AuNPs [238], AuNRs, Au nanocages, and Au nanostars are photoresistant and stable, thus offering long-time operation for optical imaging, owing to their unique interaction process with light particles showing efficient contrast in optical imaging. The most important factors in vivo diagnostic techniques include light scattering imaging, two-photon fluorescence imaging, and photothermal/photoacoustic imaging [22]. The Au nanoshells developed by Halas and co-workers that scatter light in the NIR physiological "water window" have been used as contrast agents for dark-field scattering [162, 229], photoacoustic imaging [162], and optical coherence tomography (OCT) [162, 231].

AuNPs strongly scatter light of their plasmon wavelengths. AuNRs having strong scattering in the NIR region are capable of detecting cancer cells under excitation at spectral wavelengths where biological tissues absorb only slightly (Fig. 3.14) [141]. For other imaging techniques, AuNRs can greatly enhance the contrast in the photo acoustic tomography (PAT) technique due to the high

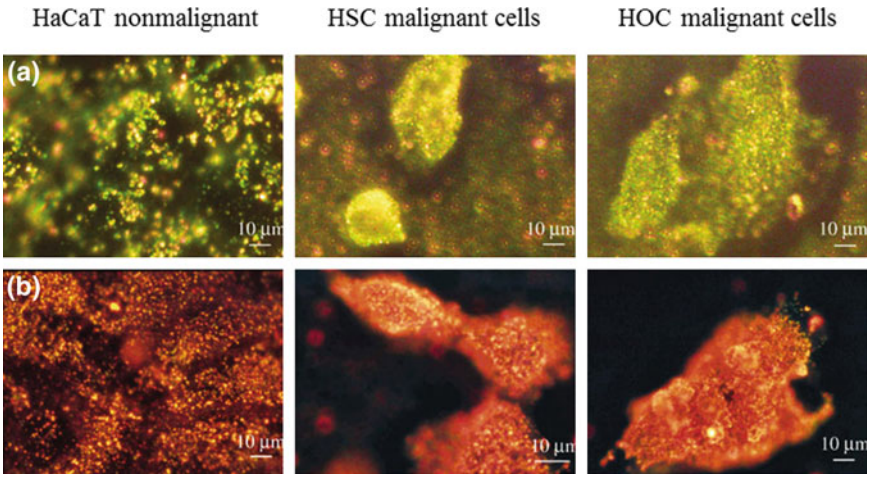

Fig. 3.14 Cancer diagnostics using AuNR-enhanced light scattering. Optical dark-field microscopy of normal HaCaT cells and cancerous HSC and HOC cells incubated with anti-EGFR antibody conjugated gold nanospheres (*top panels*, *left* to *right*). *Bottom*, as above, but with AuNRs. Anti-EGFR-conjugated gold nanoparticles specifically bound to cancer cells, thereby resulting in strong scattering under dark-field microscopy and thus enabling detection of malignant cells. **a** Light scattering images of anti-EGFR/Au nanospheres after incubation with cells for 30 min at room temperature. **b** Light scattering images of anti-EGFR/Au nanorods after incubation with cells for 30 min at room temperature [141]. Copyright 2006 American Chemical Society

efficiency of the surface plasmon absorption in the NIR region for opto-acoustic imaging [239]. For example, Etanercept-conjugated AuNRs were able to show PAT imaging of a rat tail joint [240] and this technique can be used for detecting prostate cancer [241]. Currently, dark-field imaging based on the light-scattering properties of anisotropic AuNPs (shells, spheres, rods, and cages) is widely used for cancer imaging through functionalized nanoparticle–receptor binding to cell-surface biomarkers [22, 242]. Compared with Au nanoshells, the AuNCs appear to be more effective contrast enhancement agents [243].

3.4.4.2 Photothermal Therapy

Using photothermal effect, there are applications of AuNPs for thermal therapy, drug/gene delivery. Thermal therapy involves the destruction of cancer cells by heating. Taking AuNRs as an example, they can release heat during relaxation after irradiated by laser pulse [141, 244]. When activated by a NIR laser which can penetrate cells or tissues without damage, AuNRs with low aspect ratio can be used as therapy agents to treat tumor cells in vitro based on such photothermal effect [141]. Various energy sources have been applied, including radio frequencies, high-intensity focused ultrasound, microwaves, and lasers. The heat energy can be delivered by external or internal manners, through interstitial, intraluminal, or intracavitary approaches. However, because of absorption by normal tissues, the amount of energy delivered to the treatment volume is limited, which reduces the potency of the thermal effect. To improve the efficacy and tumor selectivity, light-absorbing materials (known as photothermal contrast agents) are introduced into tumor cells to mediate the photothermal effect. A temperature increase of 30–35 °C provokes cell death. Various Au nanostructures, including nanoshells [245], NRs, NCs, and nanostars that absorb NIR light (wavelength 700–850 nm), have been shown to be effective in photothermal therapy [246]. The first use of anisotropic AuNPs in targeted photothermal therapy was conducted by the Halas research group by using silica@Au nanoshells functionalized with antibodies such as anti-HER2. The antibodies directed the AuNPs toward the cancer cells because they could conjugate with surface cell markers that were overexpressed by cancer cells. These antibodies were linked to orthopyridyl disulfide-PEG-*n*-hydrosuccinimide (OPSS-PEG-NHS) that was bound to the Au surface through strong Au–S bonds. The advantage of the PEG linker is that it provides an enhanced permeability and retention effect which involves the new blood vessels formed at the tumor site. This photothermal therapy was first demonstrated in mice with subcutaneous tumors of 1 cm size. Analysis showed that photothermal treatment resulted in tissue damage over a similar sized area as that was exposed to laser irradiation. Magnetic resonance thermal imaging (MRTI) revealed an average temperature increase of 37 °C after 5 min irradiation, which is sufficient to induce irreversible tissue damage. Nanoshell-free samples showed an average increase of 9 °C, which was considered to be safe for cell viability [247].

AuNRs have been extensively applied in this research recently. El-Sayed and coworkers pioneered strategies in utilizing AuNRs in photothermal therapy. In an

example of preferential AuNR binding to human oral cancer cells, conjugation of AuNRs to anti-EGFR antibodies could enable selective photothermal therapy [141]. In more-recent studies, they linked macrolide to PEG-functionalized AuNRs, which preferentially delivered AuNRs into inflamed tumor tissues via tumor-associated macrophage cells (TAMs) [248]. AuNRs coated by mPEG-SH 5000 could be activated by 808 nm laser with an energy of 1 W/cm^2 for 10 min and then effectively stopped the growing of mice tumors [249]. The photothermal heat generated by laser irradiated AuNRs in cells can be calculated [250]. In addition, it is noteworthy to point out in the case of pulse laser irradiation, it could induce cell death, while successive irradiation causes reshaping of the nanorods into nanospheres, thereby preventing the cell death [251]. Their promising function in photothermal therapy has the potential to replace conventional surgery and chemotherapy [252].

AuNCs with large absorption cross-sections also show a large photothermal effect. The absorbed photons are converted into phonons (lattice vibrations), which in turn produce a localized temperature increase. Xia and co-workers demonstrated the photothermal destruction of breast cancer cells in vitro through the use of immuno-AuNCs. AuNCs with an edge length of 45 nm were selected because of their predicted large absorption cross-section. SK-BR-3 cells were treated with these immuno-AuNCs, and then irradiated by a laser with a wavelength of 810 nm and a power density of 1.5 Wcm^{-2} for 5 min. The treated cells were stained with calcein-AM and ethidium homodimer-1, so that live cells showed green fluoresce and dead cells showed red fluoresce. This analysis revealed a well-defined zone of cellular death consistent with the size of the laser spot [253]. Au nanostars were successfully conjugated with anti-HER2 nanobodies and demonstrated specific interaction with HER2t and SKOV3 cells and the conjugates resulted in specific photothermal destruction of tumor cells in vitro. Exposing the cells to either only NIR light or nanoparticles did not affect cell viability. Nonspecific NPs conjugated with anti-PSA nanobodies did not result in any cell death upon laser irradiation, thus demonstrating the high specificity of these anti-HER2-conjugated Au nanostars [107]. Hybrid nanomaterials composed of two unique components not only retain the beneficial features of both, but also show synergistic properties. Hybrid AuNCs were also investigated in photothermal therapy. Single-wall carbon nanotubes (SWCNTs) were functionalized and attached to AuNCs through a thiol group. The as-prepared AuNC-decorated SWCNTs were then modified with RNA aptamer A9, which is specific to human prostate cancer cells. The photothermal response for the hybrid nanomaterial is much higher than that for single nanomaterials [254].

3.4.4.3 Drug and Gene Delivery

Anisotropic AuNPs have recently been used as nanocarriers for effective drug or gene delivery systems [255, 256]. Generally, surface functionalized AuNRs work as plasmonic carriers that simultaneously exhibit carrier capabilities, improved colloidal stability, plasmonic properties, and non-cytotoxicity under physiological

conditions. Critically, the surface of AuNRs can adsorb cargos such as DNA oligonucleotides, RNA oligonucleotides, and siRNA [238]. For the mechanism that how this system works, since there is shape transformation of AuNRs under exposure to NIR laser pulses, AuNRs are used to release DNA or drugs [257]. The AuNRs assisted gene delivery approach has caught much attention in recent years because they can replace the conventional virus-mediated gene delivery to avoid the risk of cytotoxicity and immunologic responses. For example, thiolated gene having enhanced green fluorescence protein (EGFP) was covalently conjugated to AuNRs and exposed to Q-switched Nd:YLF laser. The laser induced both of AuNR shape transformation and DNA release due to Au–S bond breakage (Fig. 3.15) [257]. During laser irradiation, the intensity of the longitudinal LSPR absorption peak at 782 nm decreased and the transverse LSPR at 520 nm increased, suggesting the transition from rod shape to spherical shape. The irradiated cells showed strong gene expression after 1–2 days, whereas in nonirradiated cells there was no gene expression. Besides thiols, Plasmid DNA was adsorbed to phosphatidylcholine (PC)-modified AuNRs by electrostatic interaction which was release by Q-switched Nd:YAG laser illumination [258]. For the result, 1 % of the DNA molecules was released and 0.5 % was active [255].

With AuNRs, the remote control of gene expression with an optical switch is accomplished. Drug delivery can also be activated under NIR laser irradiation based on AuNRs functionalized with polymer materials, such as typical poly(*N*-isopropylacrylamide) (PNIPAM) as well as its acrylic acid forms [259], due to their prominent thermal responsive properties. When temperature increases above the lower critical solution temperature (LCST), the polymer layer undergoes shrinkage. Laser irradiation induces the AuNRs to produce heat that affects the surface temperature-responsive polymer materials. By electrostatic interactions, both AuNRs and drug molecules are loaded inside the particles. When irradiated by laser, the heating energy by AuNRs triggers the microgel to deswell and release drug molecules. Further when the laser is turned off, the microgel will swell back to its original volume, thus the drug release can be controlled. Figure 3.16 illustrates the process of such laser irradiation controlled volume phase transition of AuNRs embedded PNIPAAM-hydrogels [260]. In the system, PEG modified AuNRs were first prepared

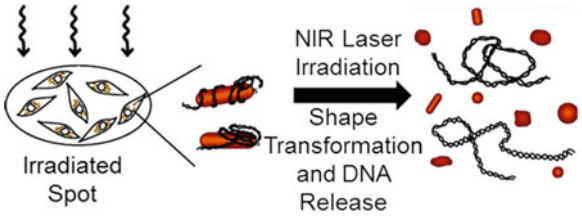

Fig. 3.15 Schematic illustration demonstrating that the cells containing EGFP-AuNR conjugates within a spot (3.5 mm in diameter) are irradiated by NIR laser (*left*). After laser irradiation, the gold nanorods of EGFP-AuNR conjugates undergo shape transformation that resulted in the release of EGFP DNA (*right*) [257]. Copyright 2006 American Chemical Society

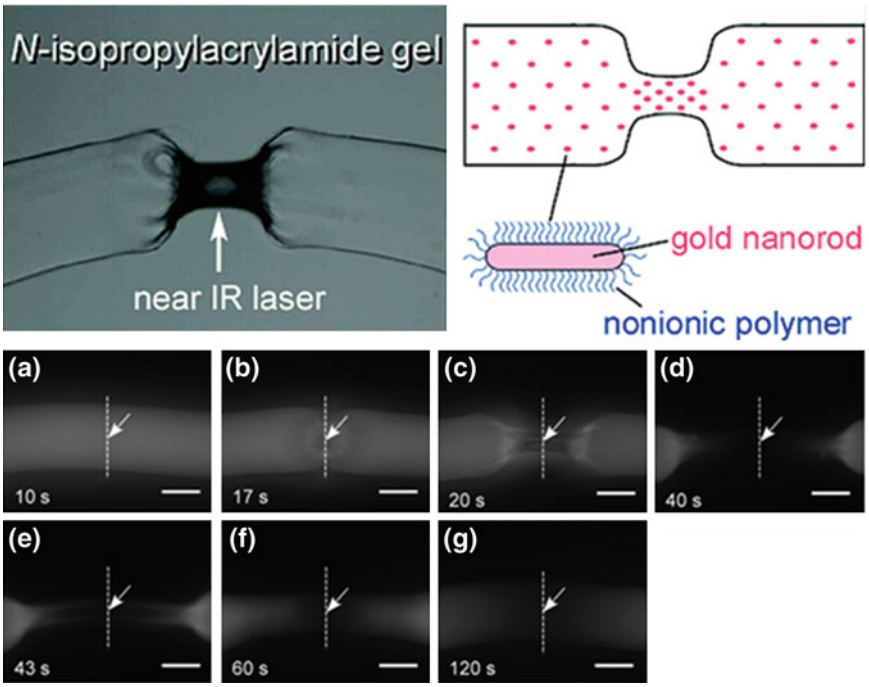

Fig. 3.16 *Top* The collapse of polymer with temperature above its LCST when under IR laser. *Bottom* **a**–**g** Fluorescence microscopic images of the polymer containing AuNRs and R-Dex-1 which has fluorescence during NIR irradiation. *Scale bars* 100 μm [260]. Copyright 2007 American Chemical Society

and then dispersed in PNIPAAM hydrogels, with concentration more than 100 μM. When stimulated by the NIR irradiation with power >490 mW, cylindrical shape gel (original diameter: 140 μm) showed shrinkage at the irradiated spot which further grew along the gel. This induced gel shrinking occurred much more rapidly by NIR irradiation than by temperature increasing. The process was monitored by the fluorescence microscope as the drug molecules (R-Dex-1) showing fluorescence pictured deformation of the gel. With the advantage of the high spatial resolution and rapid release at the irradiated spot, controlled release at the specific point of the drug was successfully achieved [260]. One attractive aspect of functional AuNRs is that they can have these applications simultaneously with proper surface materials. This is also a field for future research. In another example, AuNR/poly(*N*-isoproylacrylamide) core/shell can release norvancomycin under NIR laser irradiation [261].

Halas and co-workers described a SiO_2@Au nanoshell system that released single-stranded DNA from its surface when illuminated with plasmon-resonant light. This system allowed examination of DNA dehybridization induced by excitation of localized surface plasmons on the NPs [262]. In another study, the light-triggered release of the fluorescent molecule DAPI (4,6-diamidino-2-phenylindole) inside living cells was investigated from a host–guest complex with DNA

bound to SiO_2@Au nanoshells [263]. Diagnostic and therapeutic drug delivery based on SiO_2@Au nanoshells was also investigated recently for the treatment of ovarian cancer [264]. With their hollow structures, AuNCs serve as "pockets" that are appropriate for drug release. PEG-coated AuNCs have been used as nanocarriers for doxorubicin and triggered drug release under irradiation with NIR light. This drug delivery system was considered to be a dual-modality cancer therapy that combined both photothermal therapy and chemotherapy. An in vivo study of this delivery system indicated greater antitumor activity than either doxorubicin or AuNCs alone [246]. In another example, AuNCs coated with a thin monolayer of temperature sensitive PNIPAAm and acrylamide (Am) precursors with disulfide groups have been used for triggering release with NIR light. The IR light can be absorbed by the nanocage and converted into heat, triggering the smart polymer to collapse and release the drug payload. When the laser is turned off, the polymer chains will revert to the extended conformation and terminate the release (Fig. 3.17) [265]. The surface of AuNCs was functionalized with thermally responsive polymers to control the release through NIR laser irradiation or high-intensity focused ultrasound. Another system to achieve the controlled release was obtained using a phase-change material (PCM) loaded in the hollow interiors of AuNCs. An increase in temperature uncaps the pores and releases the guest molecules from the AuNCs. The release is controlled by varying the power or duration of the ultrasound treatment [266]. Very recently, Wan and co-workers reported a bioresponsive controlled-release AuNC system. The AuNC was selected as a support and an ATP molecule was used as the target [267].

3.4.5 Optical Tuning

Since AuNRs can provide intensive local electromagnetic fields and large field enhancements [268], there are impressive nonlinear properties leading to applications such as optical devices [269]. AuNRs show important potential in metamaterials, e.g. negative index materials for super lenses and invisible cloaking. For example, the well-organized AuNRs including self-assembly and orientations are demanded [270]. According to the design based on coordinate transformation, AuNRs self-assemble in head-to-head fashion forming continuous strips are good candidate for an optical cloak in visible frequency (Fig. 3.18). The AuNR strips are all perpendicular to the cylinder's inner and outer interfaces. For easier material generation, AuNR spatial position does not have to be periodic and can be random, and for large-scale cloaks the wires can be broken into smaller pieces that are smaller in size than the incoming wavelength. In addition, to accomplish the above materials, the fabrication techniques with controls over spacing, aspect ratio, and orientation are also important [11].

AuNWs have potential applications as nanoscale optical waveguides in the visible and NIR regions [271]. AuNWs are indeed an ideal platform to produce surface plasmon waves by direct illumination of one end of the nanostructure. They

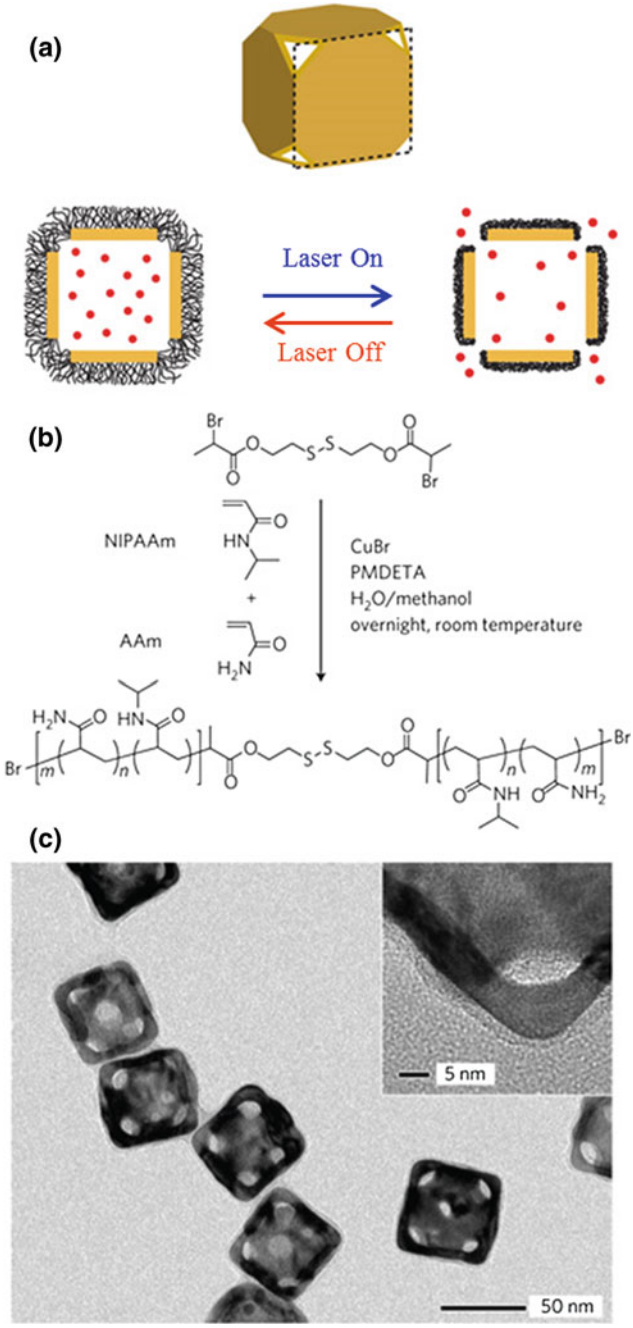
(a)
Laser On
Laser Off
(b)
NIPAAm
AAm
CuBr
PMDETA
H2O/methanol
overnight, room temperature
(c)
5 nm
50 nm

◀ **Fig. 3.17** Schematic illustration and characterization of controlled-release system by AuNCs. **a** How the system works. A side view of the Au nanocage is used for the illustration; **b** atom-transfer radical polymerization of NIPAAm and AAm monomers (at a molar ratio of m = n) as initiated by a disulphide initiator and in the presence of a Cu(I) catalyst; **c** TEM images of Au nanocages for which the surface was covered by a pNIPAAm-co-pAAm copolymer with an LSCT at 39 °C. The *inset* shows a magnified TEM image of the *corner* of such a nanocage [265]. Copyright 2009 Nature group

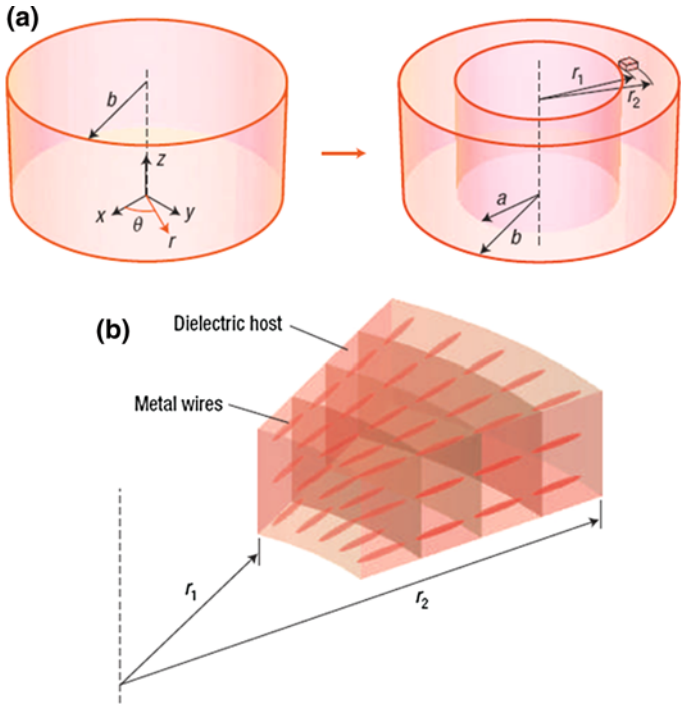

Fig. 3.18 Coordinate transformation and structure of the non-magnetic optical cloak. **a** The coordinate transformation that compresses a cylindrical region r < b into a concentric cylindrical shell a < r < b. r_1 and r_2 define the internal and external radius of a fraction of the cylindrical cloak. There is no variation along the z direction. **b** A small fraction of the cylindrical cloak showing well-organized AuNR wires [270]. Copyright 2007 Nature Group

can thus be used as tools for fundamental studies of subwavelength plasmon-based optics of wave propagation. This strategy was pioneered by Halas and co-workers, who used Ag- and Au-NWs with longitudinal dimensions of more than 10 μm. The addition of an adjacent NWs, substrate, or other symmetry-breaking defect enables direct coupling with the guided waves in a NW. Networks of plasmonic AuNWs can serve as the basis for optical devices such as interferometric logic gates, which can lead to nanorouters and multiplexes, light modulators, and a complete set of Boolean logic functions [272]. For AuNPs with branched structure such as

nanostars, it greatly increases the overall excitation cross-section and field enhancement of the nanostar tips. The antenna effect of the nanostar core may be responsible for the relatively bright and narrow scattering spectra of nanostars in the single particle measurements [273].

3.5 Conclusions and Outlook

After an extensive research in spherical AuNPs in last decades, enabled by versatile synthesis method the anisotropic AuNPs have emerged as a hot topic in recent years showing an impressive potential in applications including catalysis, sensors, biomedical uses (bioimaging, therapy, drug delivery), and optical devices. Bottom-up chemical and top-down physical approaches have been effective to provide anisotropic AuNPs with different shapes and sizes based on the knowledge of the key roles of some stabilizers such as CTAB, Ag^+, and halide ions. However, large-scale reproducible production of AuNPs of specific shapes and sizes remains a crucial challenge although such controllability has been envisioned to open up numerous opportunities for these intriguing anisotropic functional nanoscale building blocks.

Anisotropic AuNPs exhibit superior and unique optical and catalytic properties compared to their isotropic spherical counterparts [206]. They display tunable LSPR depending on their size, shape, the dielectric properties of the surrounding medium, and the self-assembly state. The LSPR band of anisotropic AuNPs can shift to the NIR region (usually 800–1300 nm) while that of spherical isotropic AuNPs position in the visible region. In the NIR region, the absorption by cells and tissues is lower, therefore the biomedical applications, including cell imaging, sensing, cancer diagnosis and treatment, and optical controlled drug and gene delivery become possible. Through suitable surface modifications, anisotropic AuNPs have been rendered biocompatible thus significantly widening their scope. Another important aspect is the emergence of metamaterials that can be fabricated from the assemblies of anisotropic AuNPs. Moreover, the applications of AuNRs and AuNWs have been demonstrated in plasmon waveguides and optical devices. Development of methods toward dynamic ordered assemblies of anisotropic AuNPs could furnish reconfigurable functional materials and devices which exploit their electronic and optical properties. Judging from the research and development progress of the anisotropic AuNPs, it can be optimistically anticipated that they will play a greater role in the nanoscience and nanotechnology of twenty-first century besides their biological and biomedical applications.

Acknowledgments The preparation of this chapter benefited from the support to Quan Li by US Air Force Office of Scientific Research (AFOSR), US Department of Energy (DOE), US Army Research Office (ARO), US Department of Defense Multidisciplinary University Research Initiative (DoD MURI), US National Aeronautics and Space Administration (NASA), and US National Science Foundation (NSF), and Ohio Third Frontier.

References

1. I. Freestone, N. Meeks, M. Sax, C. Higgitt, The lycurgus cup-a roman nanotechnology. Gold Bull. **40**, 270–277 (2007)
2. A.P. Alivisatos, Semiconductor clusters, nanocrystals, and quantum dots. Science **271**, 933–937 (1996)
3. P. Mulvaney, Surface plasmon spectroscopy of nanosized metal particles. Langmuir **12**, 788–800 (1996)
4. S. Lal, S.E. Clare, N.J. Halas, Nanoshell-enabled photothermal cancer therapy: impending clinical impact. Acc. Chem. Res. **41**, 1842–1851 (2008)
5. C.J. Murphy, A.M. Gole, J.W. Stone, P.N. Sisco, A.M. Alkilany, E.C. Goldsmith, S.C. Baxter, Gold nanoparticles in biology: beyond toxicity to cellular imaging. Acc. Chem. Res. **41**, 1721–1730 (2008)
6. C. Burda, X.B. Chen, R. Narayanan, M.A. El-Sayed, Chemistry and properties of nanocrystals of different shapes. Chem. Rev. **105**, 1025–1102 (2005)
7. Y. Yin, A.P. Alivisatos, Colloidal nanocrystal synthesis and the organic-inorganic interface. Nature **437**, 664–670 (2005)
8. N.J. Halas, S. Lal, W.S. Chang, S. Link, P. Nordlander, Plasmons in strongly coupled metallic nanostructures. Chem. Rev. **111**, 3913–3961 (2011)
9. L. Billot, M.L. de la Chapelle, A.S. Grimault, A. Vial, D. Barchiesi, J.L. Bijeon, P.M. Adam, P. Royer, Surface enhanced Raman scattering on gold nanowire arrays: evidence of strong multipolar surface plasmon resonance enhancement. Chem. Phys. Lett. **422**, 303–307 (2006)
10. E.J. Smythe, E. Cubukcu, F. Capasso, Optical properties of surface plasmon resonances of coupled metallic nanorods. Opt. Express **15**, 7439–7447 (2007)
11. E. Cubukcu, E.A. Kort, K.B. Crozier, F. Capasso, Plasmonic laser antenna. Appl. Phys. Lett. **89**, 093120 (2006)
12. A.N. Grigorenko, N.W. Roberts, M.R. Dickinson, Y. Zhang, Nanometric optical tweezers based on nanostructured substrates. Nat. Photon. **2**, 365–370 (2008)
13. E. Devaux, T.W. Ebbesen, J.C. Weeber, A. Dereux, Launching and decoupling surface plasmons via micro-gratings. Appl. Phys. Lett. **83**, 4936–4938 (2003)
14. W.L. Barnes, A. Dereux, T.W. Ebbesen, Surface plasmon subwavelength optics. Nature **424**, 824–830 (2003)
15. B.J.Y. Tan, C.H. Sow, T.S. Koh, K.C. Chin, A.T.S. Wee, C.K. Ong, Fabrication of size-tunable gold nanoparticles array with nanosphere lithography, reactive ion etching, and thermal annealing. J. Phys. Chem. B **109**, 11100–11109 (2005)
16. D.D. Jia, A. Goonewardene, Two-dimensional nanotriangle and nanoring arrays on silicon wafer. Appl. Phys. Lett. **88**, 053105 (2006)
17. L.D. Qin, S. Park, L. Huang, C.A. Mirkin, On-wire lithography. Science **309**, 113–115 (2005)
18. L. Qin, S. Zou, C. Xue, A. Atkinson, G.C. Schatz, C.A. Mirkin, Designing, fabricating, and imaging Raman hot spots. Proc. Natl. Acad. Sci. USA **103**, 13300–13303 (2006)
19. K.D. Osberg, A.L. Schmucker, A.J. Senesi, C.A. Mirkin, One-dimensional nanorod arrays: independent control of composition, length, and interparticle spacing with nanometer precision. Nano Lett. **11**, 820–824 (2011)
20. R.S. Wagner, W.C. Ellis, Vapor-liquid-solid mechanism of single crystal growth. Appl. Phys. Lett. **4**, 89–90 (1964)
21. J. Wiesner, A. Wokaun, Anisometric gold colloids-preparation, characterization, and optical-properties. Chem. Phys. Lett. **157**, 569–575 (1989)
22. E.C. Dreaden, A.M. Alkilany, X. Huang, C.J. Murphy, M.A. El-Sayed, The golden age: gold nanoparticles for biomedicine. Chem. Soc. Rev. **41**, 2740–2779 (2012)
23. C.J. Murphy, A.M. Gole, S.E. Hunyadi, C.J. Orendorff, One-dimensional colloidal gold and silver nanostructures. Inorg. Chem. **45**, 7544–7554 (2006)

24. B. Nikoobakht, M.A. El-Sayed, Preparation and growth mechanism of gold nanorods (NRs) using seed-mediated growth method. Chem. Mater. **15**, 1957–1962 (2003)
25. J. Zhang, M.R. Langille, M.L. Personick, K. Zhang, S. Li, C.A. Mirkin, Concave cubic gold nanocrystals with high-index facets. J. Am. Chem. Soc. **132**, 14012–14014 (2010)
26. M. Iqbal, Y.I. Chung, G. Tae, An enhanced synthesis of gold nanorods by the addition of Pluronic (F-127) via a seed mediated growth process. J. Mater. Chem. **17**, 335–342 (2007)
27. B.D. Busbee, S.O. Obare, C.J. Murphy, An improved synthesis of high-aspect-ratio gold nanorods. Adv. Mater. **15**, 414–416 (2003)
28. N.R. Jana, L. Gearheart, C.J. Murphy, Wet chemical synthesis of high aspect ratio cylindrical gold nanorods. J. Phys. Chem. B **105**, 4065–4067 (2001)
29. C.J. Murphy, T.K. San, A.M. Gole, C.J. Orendorff, J.X. Gao, L. Gou, S.E. Hunyadi, T. Li, Anisotropic metal nanoparticles: synthesis, assembly, and optical applications. J. Phys. Chem. B **109**, 13857–13870 (2005)
30. T.K. Sau, C.J. Murphy, Seeded high yield synthesis of short Au nanorods in aqueous solution. Langmuir **20**, 6414–6420 (2004)
31. N. Garg, C. Scholl, A. Mohanty, R. Jin, The role of bromide ions in seeding growth of au nanorods. Langmuir **26**, 10271–10276 (2010)
32. N.R. Jana, Gram-scale synthesis of soluble, near-monodisperse gold nanorods and other anisotropic nanoparticles. Small **1**, 875–882 (2005)
33. R.A. Alvarez-Puebla, A. Agarwal, P. Manna, B.P. Khanal, P. Aldeanueva-Potel, E. Carbo-Argibay, N. Pazos-Perez, L. Vigderman, E.R. Zubarev, N.A. Kotov, L.M. Liz-Marzan, Gold nanorods 3D-supercrystals as surface enhanced Raman scattering spectroscopy substrates for the rapid detection of scrambled prions. Proc. Natl. Acad. Sci. USA **108**, 8157–8161 (2011)
34. L.L. Feng, X.C. Wu, L.R. Ren, Y.J. Xiang, W.W. He, K. Zhang, W.Y. Zhou, S.S. Xie, Well-controlled synthesis of Au@Pt nanostructures by gold-nanorod-seeded growth. Chem. Eur. J. **14**, 9764–9771 (2008)
35. J.H. Song, F. Kim, D. Kim, P.D. Yang, Crystal overgrowth on gold nanorods: tuning the shape, facet, aspect ratio, and composition of the nanorods. Chem. Eur. J. **11**, 910–916 (2005)
36. E. Carbo-Argibay, B. Rodriguez-Gonzalez, J. Pacifico, I. Pastoriza-Santos, J. Perez-Juste, L. M. Liz-Marzan, Chemical sharpening of gold nanorods: the rod-to-octahedron transition. Angew. Chem. Int. Ed. **46**, 8983–8987 (2007)
37. X.S. Kou, S.Z. Zhang, Z. Yang, C.K. Tsung, G.D. Stucky, L.D. Sun, J.F. Wang, C.H. Yan, Glutathione- and cysteine-induced transverse overgrowth on gold nanorods. J. Am. Chem. Soc. **129**, 6402–6404 (2007)
38. S.E. Lohse, C.J. Murphy, The quest for shape control: a history of gold nanorod synthesis. Chem. Mater. **25**, 1250–1261 (2013)
39. N. Li, P.X. Zhao, D. Astruc, Anisotropic gold nanoparticles: synthesis, properties, applications, and toxicity. Angew. Chem. Int. Ed. **53**, 1756–1789 (2014)
40. K. Esumi, K. Matsuhisa, K. Torigoe, Preparation of rodlike gold particles by uv irradiation using cationic micelles as a template. Langmuir **11**, 3285–3287 (1995)
41. F. Kim, J.H. Song, P.D. Yang, Photochemical synthesis of gold nanorods. J. Am. Chem. Soc. **124**, 14316–14317 (2002)
42. E. Leontidis, K. Kleitou, T. Kyprianidou-Leodidou, V. Bekiari, P. Lianos, Gold colloids from cationic surfactant solutions. 1. Mechanisms that control particle morphology. Langmuir **18**, 3659–3668 (2002)
43. S. Eustis, H.Y. Hsu, M.A. El-Sayed, Gold nanoparticle formation from photochemical reduction of Au^{3+} by continuous excitation in colloidal solutions. A proposed molecular mechanism. J. Phys. Chem. B **109**, 4811–4815 (2005)
44. C.Y. Wang, C. Y. Liu, X. Zheng, J. Chen, T. Shen, The surface chemistry of hybrid nanometer-sized particles-I. Photochemical deposition of gold on ultrafine TiO_2 particles. Colloids Surf. A **131**, 271–280 (1998)

45. G.L. Hornyak, C.J. Patrissi, C.R. Martin, Fabrication, characterization, and optical properties of gold nanoparticle/porous alumina composites: the nonscattering Maxwell-Garnett limit. J. Phys. Chem. B **101**, 1548–1555 (1997)
46. J.C. Hulteen, C.R. Martin, A general template-based method for the preparation of nanomaterials. J. Mater. Chem. **7**, 1075–1087 (1997)
47. Y.Y. Yu, S.S. Chang, C.L. Lee, C.R.C. Wang, Gold nanorods: electrochemical synthesis and optical properties. J. Phys. Chem. B **101**, 6661–6664 (1997)
48. Z.L. Wang, R.P. Gao, B. Nikoobakht, M.A. El-Sayed, Surface reconstruction of the unstable 110 surface in gold nanorods. J. Phys. Chem. B **104**, 5417–5420 (2000)
49. W. Ye, J. Yan, Q. Ye, F. Zhou, Template-free and direct electrochemical deposition of hierarchical dendritic gold microstructures: growth and their multiple applications. J. Phys. Chem. C **114**, 15617–15624 (2010)
50. K. Barbour, M. Ashokkumar, R.A. Caruso, F. Grieser, Sonochemistry and sonoluminescence in aqueous $AuCl_4^-$ solutions in the presence of surface-active solutes. J. Phys. Chem. B **103**, 9231–9236 (1999)
51. J.L. Zhang, J.M. Du, B.X. Han, Z.M. Liu, T. Jiang, Z.F. Zhang, Sonochemical formation of single-crystalline gold nanobelts. Angew. Chem. Int. Ed. **45**, 1116–1119 (2006)
52. T. Pham, J.B. Jackson, N.J. Halas, T.R. Lee, Preparation and characterization of gold nanoshells coated with self-assembled monolayers. Langmuir **18**, 4915–4920 (2002)
53. N. Taub, O. Krichevski, G. Markovich, Growth of gold nanorods on surfaces. J. Phys. Chem. B **107**, 11579–11582 (2003)
54. A.J. Mieszawska, F.P. Zamborini, Gold nanorods grown directly on surfaces from microscale patterns of gold seeds. Chem. Mater. **17**, 3415–3420 (2005)
55. J. Henzie, E.S. Kwak, T.W. Odom, Mesoscale metallic pyramids with nanoscale tips. Nano Lett. **5**, 1199–1202 (2005)
56. G.M. Lu, R. Zhao, G. Qian, Y.X. Qi, X.L. Wang, J.S. Suo, A highly efficient catalyst Au/MCM-41 for selective oxidation cyclohexane using oxygen. Catal. Lett. **97**, 115–118 (2004)
57. R.M. Penner, Mesoscopic metal particles and wires by electrodeposition. J. Phys. Chem. B **106**, 3339–3353 (2002)
58. V.M. Cepak, C.R. Martin, Preparation and stability of template-synthesized metal nanorod sols in organic solvents. J. Phys. Chem. B **102**, 9985–9990 (1998)
59. S.E. Skrabalak, J. Chen, L. Au, X. Lu, X. Li, Y. Xia, Gold nanocages for biomedical applications. Adv. Mater. **19**, 3177–3184 (2007)
60. Y. Zhang, H.J. Dai, Formation of metal nanowires on suspended single-walled carbon nanotubes. Appl. Phys. Lett. **77**, 3015–3017 (2000)
61. J.H. Song, Y.Y. Wu, B. Messer, H. Kind, P.D. Yang, Metal nanowire formation using Mo_3Se^{3-} as reducing and sacrificing templates. J. Am. Chem. Soc. **123**, 10397–10398 (2001)
62. J.L. Gardea-Torresdey, J.G. Parsons, E. Gomez, J. Peralta-Videa, H.E. Troiani, P. Santiago, M.J. Yacaman, Formation and growth of Au nanoparticles inside live alfalfa plants. Nano Lett. **2**, 397–401 (2002)
63. S. He, Y. Zhang, Z. Guo, N. Go, Biological synthesis of gold nanowires using extract of Rhodopseudomonas capsulata. Biotechnol. Prog. **24**, 476–480 (2008)
64. S. Brown, M. Sarikaya, E. Johnson, A genetic analysis of crystal growth. J. Mol. Biol. **299**, 725–735 (2000)
65. M.Q. Zhao, R.M. Crooks, Intradendrimer exchange of metal nanoparticles. Chem. Mater. **11**, 3379–3385 (1999)
66. M.F. Mrozek, Y. Xie, M.J. Weaver, Surface-enhanced Raman scattering on uniform platinum-group overlayers: preparation by redox replacement of underpotential-deposited metals on gold. Anal. Chem. **73**, 5953–5960 (2001)
67. L. Au, X. Lu, Y. Xia, A comparative study of galvanic replacement reactions involving Ag nanocubes and $AuCl_2^-$ or $AuCl_4^-$. Adv. Mater. **20**, 2517–2522 (2008)

68. Y.G. Sun, Y. Xia, Mechanistic study on the replacement reaction between silver nanostructures and chloroauric acid in aqueous medium. J. Am. Chem. Soc. **126**, 3892–3901 (2004)
69. Q. Xu, G. Meng, X. Wu, Q. Wei, M. Kong, X. Zhu, Z. Chu, A generic approach to desired metallic nanowires inside native porous alumina template via redox reaction. Chem. Mater. **21**, 2397–2402 (2009)
70. W. Ye, Y. Chen, F. Zhou, C. Wang, Y. Li, Fluoride-assisted galvanic replacement synthesis of Ag and Au dentrites on aluminum foil with enhanced SERS and catalytic activities. J. Mater. Chem. **22**, 18327–18334 (2012)
71. A. Paul, D. Solis Jr, K. Bao, W.-S. Chang, S. Nauert, L. Vidgerman, E.R. Zubarev, P. Nordlander, S. Link, Identification of higher order long-propagation-length surface plasmon polariton modes in chemically prepared gold nanowires. ACS Nano **6**, 8105–8113 (2012)
72. J.U. Kim, S.H. Cha, K. Shin, J.Y. Jho, J.C. Lee, Preparation of gold nanowires and nanosheets in bulk block copolymer phases under mild conditions. Adv. Mater. **16**, 459–464 (2004)
73. C.C. Mayorga-Martinez, M. Guix, R.E. Madrid, A. Merkoci, Bimetallic nanowires as electrocatalysts for nonenzymatic real-time impedancimetric detection of glucose. Chem. Commun. **48**, 1686–1688 (2012)
74. Z. Jiang, Q. Zhang, C. Zong, B.-J. Liu, B. Ren, Z. Xie, L. Zheng, Cu-Au alloy nanotubes with five-fold twinned structure and their application in surface-enhanced Raman scattering. J. Mater. Chem. **22**, 18192–18197 (2012)
75. M. Wirtz, C.R. Martin, Template-fabricated gold nanowires and nanotubes. Adv. Mater. **15**, 455–458 (2003)
76. F. Muench, U. Kunz, C. Neetzel, S. Lauterbach, H.-J. Kleebe, W. Ensinger, 4-(Dimethylamino)pyridine as a powerful auxiliary reagent in the electroless synthesis of gold nanotubes. Langmuir **27**, 430–435 (2011)
77. N.R. Sieb, N.-C. Wu, E. Majidi, R. Kukreja, N.R. Branda, B.D. Gates, Hollow metal nanorods with tunable dimensions, porosity, and photonic properties. ACS Nano **3**, 1365–1372 (2009)
78. C.R. Bridges, P.M. DiCarmine, D.S. Seferos, Gold nanotubes as sensitive, solution-suspendable refractive index reporters. Chem. Mater. **24**, 963–965 (2012)
79. J.-H. Ryu, S. Park, B. Kim, A. Klaikherd, T.P. Russell, S. Thayumanavan, Highly ordered gold nanotubes using thiols at a cleavable block copolymer interface. J. Am. Chem. Soc. **131**, 9870–9871 (2009)
80. M. Grzelczak, A. Sanchez-Iglesias, H.H. Mezerji, S. Bals, J. Perez-Juste, L.M. Liz-Marzan, Steric hindrance induces crosslike self-assembly of gold nanodumbbells. Nano Lett. **12**, 4380–4384 (2012)
81. M. Grzelczak, A. Sanchez-Iglesias, B. Rodriguez-Gonzalez, R. Alvarez-Puebla, J. Perez-Juste, L.M. Liz-Marzan, Influence of iodide ions on the growth of gold nanorods: tuning tip curvature and surface plasmon resonance. Adv. Funct. Mater. **18**, 3780–3786 (2008)
82. M.F. Cardinal, B. Rodriguez-Gonzalez, R.A. Alvarez-Puebla, J. Perez-Juste, L.M. Liz-Marzan, Modulation of localized surface plasmons and SERS response in gold dumbbells through silver coating. J. Phys. Chem. C **114**, 10417–10423 (2010)
83. W. Xie, L. Su, P. Donfack, A. Shen, X. Zhou, M. Sackmann, A. Materny, J. Hu, Synthesis of gold nanopeanuts by citrate reduction of gold chloride on gold-silver core-shell nanoparticles. Chem. Commun. **35**, 5263–5265 (2009)
84. E. Shaviv, U. Banin, Synergistic effects on second harmonic generation of hybrid CdSe-Au nanoparticles. ACS Nano **4**, 1529–1538 (2010)
85. G. Krylova, L.J. Giovanetti, F.G. Requejo, N.M. Dimitrijevic, A. Prakapenka, E.V. Shevchenko, Study of nucleation and growth mechanism of the metallic nanodumbbells. J. Am. Chem. Soc. **134**, 4384–4392 (2012)

86. Y. Kuroda, Y. Sakamoto, K. Kuroda, Selective cleavage of periodic mesoscale structures: two-dimensional replication of binary colloidal crystals into dimpled gold nanoplates. J. Am. Chem. Soc. **134**, 8684–8692 (2012)
87. S. Porel, S. Singh, T.P. Radhakrishnan, Polygonal gold nanoplates in a polymer matrix. Chem. Commun. **14**, 2387–2389 (2005)
88. X.P. Sun, S.J. Dong, E.K. Wang, High-yield synthesis of large single-crystalline gold nanoplates through a polyamine process. Langmuir **21**, 4710–4712 (2005)
89. B. Lim, P.H.C. Camargo, Y. Xia, Mechanistic study of the synthesis of an nanotadpoles, nanokites, and microplates by reducing aqueous $HAuCl_4$ with poly(vinyl pyrrolidone). Langmuir **24**, 10437–10442 (2008)
90. X.P. Sun, S.J. Dong, E. Wang, Large-scale synthesis of micrometer-scale single-crystalline Au plates of nanometer thickness by a wet-chemical route. Angew. Chem. Int. Ed. **43**, 6360–6363 (2004)
91. H.C. Chu, C.H. Kuo, M.H. Huang, Thermal aqueous solution approach for the synthesis of triangular and hexagonal gold nanoplates with three different size ranges. Inorg. Chem. **45**, 808–813 (2006)
92. Y. Shao, Y.D. Jin, S.J. Dong, Synthesis of gold nanoplates by aspartate reduction of gold chloride. Chem. Commun. **9**, 1104–1105 (2004)
93. B. Liu, J. Xie, J.Y. Lee, Y.P. Ting, J.P. Chen, Optimization of high-yield biological synthesis of single-crystalline gold nanoplates. J. Phys. Chem. B **109**, 15256–15263 (2005)
94. Y. Zhang, G. Chang, S. Liu, W. Lu, J. Tian, X. Sun, A new preparation of Au nanoplates and their application for glucose sensing. Biosens. Bioelectron. **28**, 344–348 (2011)
95. J. Xie, J.Y. Lee, D.I.C. Wang, Synthesis of single-crystalline gold nanoplates in aqueous solutions through biomineralization by serum albumin protein. J. Phys. Chem. C **111**, 10226–10232 (2007)
96. L. Wang, X. Wu, X. Li, L. Wang, M. Pei, X. Tao, Facile synthesis of concave gold nanoplates in hexagonal liquid crystal made of SDS/water system. Chem. Commun. **46**, 8422–8423 (2010)
97. J.E. Millstone, S.J. Hurst, G.S. Metraux, J.I. Cutler, C.A. Mirkin, Colloidal gold and silver triangular nanoprisms. Small **5**, 646–664 (2009)
98. M.R. Jones, R.J. Macfarlane, A.E. Prigodich, P.C. Patel, C.A. Mirkin, Nanoparticle shape anisotropy dictates the collective behavior of surface-bound ligands. J. Am. Chem. Soc. **133**, 18865–18869 (2011)
99. M.J. Banholzer, N. Harris, J.E. Millstone, G.C. Schatz, C.A. Mirkin, Abnormally large plasmonic shifts in silica-protected gold triangular nanoprisms. J. Phys. Chem. C **114**, 7521–7526 (2010)
100. J.Q. Hu, Y. Zhang, B. Liu, J.X. Liu, H.H. Zhou, Y.F. Xu, Y.X. Jiang, Z.L. Yang, Z.Q. Tian, Synthesis and properties of tadpole-shaped gold nanoparticles. J. Am. Chem. Soc. **126**, 9470–9471 (2004)
101. L. Huang, M. Wang, Y. Zhang, Z. Guo, J. Sun, N. Gu, Synthesis of gold nanotadpoles by a temperature-reducing seed approach and the dielectrophoretic manipulation. J. Phys. Chem. C **111**, 16154–16160 (2007)
102. P.H.C. Camargo, Y. Xiong, L. Ji, J.M. Zuo, Y. Xia, Facile synthesis of tadpole-like nanostructures consisting of Au heads and Pd tails. J. Am. Chem. Soc. **129**, 15452–15453 (2007)
103. D.Y. Kim, T. Yu, E.C. Cho, Y. Ma, O.O. Park, Y. Xia, Synthesis of gold nano-hexapods with controllable arm lengths and their tunable optical properties. Angew. Chem. Int. Ed. **50**, 6328–6331 (2011)
104. S.K. Dondapati, T.K. Sau, C. Hrelescu, T.A. Klar, F.D. Stefani, J. Feldmann, Label-free biosensing based on single gold nanostars as plasmonic transducers. ACS Nano **4**, 6318–6322 (2010)
105. H. Yuan, C.G. Khoury, H. Hwang, C.M. Wilson, G.A. Grant, V.-D. Tuan, Gold nanostars: surfactant-free synthesis, 3D modelling, and two-photon photoluminescence imaging. Nanotechnology **23**, 075102 (2012)

106. J. Xie, Q. Zhang, J.Y. Lee, D.I.C. Wang, The synthesis of SERS-active gold nanoflower tags for in vivo applications. ACS Nano **2**, 2473–2480 (2008)
107. B. Van de Broek, N. Devoogdt, A. D'Hollander, H.-L. Gijs, K. Jans, L. Lagae, S. Muyldermans, G. Maes, G. Borghs, Specific cell targeting with nanobody conjugated branched gold nanoparticles for photothermal therapy. ACS Nano **5**, 4319–4328 (2011)
108. S.H. Chen, Z.L. Wang, J. Ballato, S.H. Foulger, D.L. Carroll, Monopod, bipod, tripod, and tetrapod gold nanocrystals. J. Am. Chem. Soc. **125**, 16186–16187 (2003)
109. T.K. Sau, C.J. Murphy, Room temperature, high-yield synthesis of multiple shapes of gold nanoparticles in aqueous solution. J. Am. Chem. Soc. **126**, 8648–8649 (2004)
110. Z. Li, W. Li, P.H.C. Camargo, Y. Xia, Facile synthesis of branched an nanostructures by templating against a self-destructive lattice of magnetic fe nanoparticles. Angew. Chem. Int. Ed. **47**, 9653–9656 (2008)
111. E. Hao, R.C. Bailey, G.C. Schatz, J.T. Hupp, S.Y. Li, Synthesis and optical properties of "branched" gold nanocrystals. Nano Lett. **4**, 327–330 (2004)
112. F. Hao, C.L. Nehl, J.H. Hafner, P. Nordlander, Plasmon resonances of a gold nanostar. Nano Lett. **7**, 729–732 (2007)
113. T.H. Lin, C.W. Lin, H.H. Liu, J.T. Sheu, W.H. Hung, Potential-controlled electrodeposition of gold dentrites in the presence of cysteine. Chem. Commun. **47**, 2044–2046 (2011)
114. D. Huang, X. Bai, L. Zheng, Ultrafast preparation of three-dimensional dendritic gold nanostructures in aqueous solution and their applications in catalysis and SERS. J. Phys. Chem. C **115**, 14641–14647 (2011)
115. T. Huang, F. Meng, L. Qi, Controlled synthesis of dendritic gold nanostructures assisted by supramolecular complexes of surfactant with cyclodextrin. Langmuir **26**, 7582–7589 (2010)
116. C. Radloff, N.J. Halas, Nano Lett. **4**, 1323 (2004)
117. S.J. Oldenburg, J.B. Jackson, S.L. Westcott, N.J. Halas, Infrared extinction properties of gold nanoshells. Appl. Phys. Lett. **75**, 2897–2899 (1999)
118. L.R. Hirsch, A.M. Gobin, A.R. Lowery, F. Tam, R.A. Drezek, N.J. Halas, J.L. West, Metal nanoshells. Ann. Biomed. Eng. **34**, 15–22 (2006)
119. T. Zhou, B. Wu, D. Xing, Bio-modified Fe_3O_4 core/Au shell nanoparticles for targeting and multimodal imaging of cancer cells. J. Mater. Chem. **22**, 470–477 (2012)
120. D. Llamosa Perez, A. Espinosa, L. Martinez, E. Roman, C. Ballesteros, A. Mayoral, M. Garcia-Hernandez, Y. Huttel, Thermal diffusion at nanoscale: from CoAu alloy nanoparticles to Co@Au core/shell structures. J. Phys. Chem. C **117**, 3101–3108 (2013)
121. M.Z. Liu, P. Guyot-Sionnest, Synthesis and optical characterization of Au/Ag core/shell nanorods. J. Phys. Chem. B **108**, 5882–5888 (2004)
122. L.H. Lu, H.S. Wang, Y.H. Zhou, S.Q. Xi, H.J. Zhang, H.B.W. Jiawen, B. Zhao, Seed-mediated growth of large, monodisperse core-shell gold-silver nanoparticles with Ag-like optical properties. Chem. Commun. **21**, 144–145 (2002)
123. S.O. Obare, N.R. Jana, C.J. Murphy, Preparation of polystyrene- and silica-coated gold nanorods and their use as templates for the synthesis of hollow nanotubes. Nano Lett. **1**, 601–603 (2001)
124. A. Gole, J.W. Stone, W.R. Gemmill, H.C. zur Loye, C.J. Murphy, Iron oxide coated gold nanorods: synthesis, characterization, and magnetic manipulation. Langmuir **24**, 6232–6237 (2008)
125. M. Grzelczak, J. Perez-Juste, B. Rodriguez-Gonzalez, L.M. Liz-Marzan, Influence of silver ions on the growth mode of platinum on gold nanorods. J. Mater. Chem. **16**, 3946–3951 (2006)
126. M. Liu, P. Guyot-Sionnest, Preparation and optical properties of silver chalcogenide coated gold nanorods. J. Mater. Chem. **16**, 3942–3945 (2006)
127. F. Caruso, M. Spasova, V. Saigueirino-Maceira, L.M. Liz-Marzan, Multilayer assemblies of silica-encapsulated gold nanoparticles on decomposable colloid templates. Adv. Mater. **13**, 1090–1094 (2001)
128. Z.J. Liang, A. Susha, F. Caruso, Gold nanoparticle-based core-shell and hollow spheres and ordered assemblies thereof. Chem. Mater. **15**, 3176–3183 (2003)

129. S.E. Skrabalak, J. Chen, Y. Sun, X. Lu, L. Au, C.M. Cobley, Y. Xia, Gold nanocages: synthesis, properties, and applications. Acc. Chem. Res. **41**, 1587–1595 (2008)
130. X. Lu, L. Au, J. McLellan, Z.-Y. Li, M. Marquez, Y. Xia, Fabrication of cubic nanocages and nanoframes by dealloying Au/Ag alloy nanoboxes with an aqueous etchant based on Fe $(NO_3)_3$ or NH_4OH. Nano Lett. **7**, 1764–1769 (2007)
131. F. Kim, S. Connor, H. Song, T. Kuykendall, P.D. Yang, Platonic gold nanocrystals. Angew. Chem. Int. Ed. **43**, 3673–3677 (2004)
132. Y.G. Sun, Y.N. Xia, Shape-controlled synthesis of gold and silver nanoparticles. Science **298**, 2176–2179 (2002)
133. C. Li, K.L. Shuford, Q.H. Park, W. Cai, Y. Li, E.J. Lee, S.O. Cho, High-yield synthesis of single-crystalline gold nano-octahedra. Angew. Chem. Int. Ed. **46**, 3264–3286 (2007)
134. T.W. Hamann, N. Srivatsan, H. van Willigen, Time-resolved EPR study of the photophysics and photochemistry of 1-(3-(methoxycarbonyl)propyl)-1-phenyl[6.6]C61. J. Phys. Chem. A **109**, 11665–11672 (2005)
135. K. Kwon, K.Y. Lee, Y.W. Lee, M. Kim, J. Heo, S.J. Ahn, S.W. Han, Controlled synthesis of icosahedral gold nanoparticles and their surface-enhanced Raman scattering property. J. Phys. Chem. C **111**, 1161–1165 (2007)
136. U. Kreibig, M. Vollmer, *Optical properties of metal clusters* (Springer, Berlin, 1995)
137. S. Link, M.A. El-Sayed, Shape and size dependence of radiative, non-radiative and photothermal properties of gold nanocrystals. Int. Rev. Phys. Chem. **19**, 409–453 (2000)
138. P.K. Jain, K.S. Lee, I.H. El-Sayed, M.A. El-Sayed, Calculated absorption and scattering properties of gold nanoparticles of different size, shape, and composition: applications in biological imaging and biomedicine. J. Phys. Chem. B **110**, 7238–7248 (2006)
139. G.C. Papavassiliou, Optical-properties of small inorganic and organic metal particles. Prog. Solid State Ch. **12**, 185–271 (1979)
140. L. Qiu, T.A. Larson, D.K. Smith, E. Vitkin, S. Zhang, M.D. Modell, I. Itzkan, E.B. Hanlon, B.A. Korgel, K.V. Sokolov, L.T. Perelman, Single gold nanorod detection using confocal light absorption and scattering spectroscopy. IEEE J. Sel. Top. Quantum Electron. **13**, 1730–1738 (2007)
141. X.H. Huang, I.H. El-Sayed, W. Qian, M.A. El-Sayed, Cancer cell imaging and photothermal therapy in the near-infrared region by using gold nanorods. J. Am. Chem. Soc. **128**, 2115–2120 (2006)
142. S. Link, M.A. Ei-Sayed, Optical properties and ultrafast dynamics of metallic nanocrystals. Annu. Rev. Phys. Chem. **54**, 331–366 (2003)
143. S. Link, C. Burda, M.B. Mohamed, B. Nikoobakht, M.A. El-Sayed, Laser photothermal melting and fragmentation of gold nanorods: energy and laser pulse-width dependence. J. Phys. Chem. A **103**, 1165–1170 (1999)
144. S. Link, Z.L. Wang, M.A. El-Sayed, How does a gold nanorod melt? J. Phys. Chem. B **104**, 7867–7870 (2000)
145. M.B. Mohamed, V. Volkov, S. Link, M.A. El-Sayed, The 'lightning' gold nanorods: fluorescence enhancement of over a million compared to the gold metal. Chem. Phys. Lett. **317**, 517–523 (2000)
146. S. Link, M.A. El-Sayed, Spectral properties and relaxation dynamics of surface plasmon electronic oscillations in gold and silver nanodots and nanorods. J. Phys. Chem. B **103**, 8410–8426 (1999)
147. G. Raschke, S. Kowarik, T. Franzl, C. Sonnichsen, T.A. Klar, J. Feldmann, A. Nichtl, K. Kurzinger, Biomolecular recognition based on single gold nanoparticle light scattering. Nano Lett. **3**, 935–938 (2003)
148. X.H. Huang, S. Neretina, M.A. El-Sayed, Gold nanorods: from synthesis and properties to biological and biomedical applications. Adv. Mater. **21**, 4880–4910 (2009)
149. K.S. Lee, M.A. El-Sayed, Dependence of the enhanced optical scattering efficiency relative to that of absorption for gold metal nanorods on aspect ratio, size, end-cap shape, and medium refractive index. J. Phys. Chem. B **109**, 20331–20338 (2005)

150. L.J.E. Anderson, C.M. Payne, Y.-R. Zhen, P. Nordlander, J.H. Hafner, A tunable plasmon resonance in gold nanobelts. Nano Lett. **11**, 5034–5037 (2011)
151. P.K. Jain, W.Y. Huang, M.A. El-Sayed, On the universal scaling behavior of the distance decay of plasmon coupling in metal nanoparticle pairs: a plasmon ruler equation. Nano Lett. **7**, 2080–2088 (2007)
152. P.K. Jain, X. Huang, I.H. El-Sayed, M.A. El-Sayed, Noble metals on the nanoscale: optical and photothermal properties and some applications in imaging, sensing, biology, and medicine. Acc. Chem. Res. **41**, 1578–1586 (2008)
153. L. Xu, H. Kuang, L. Wang, C. Xu, Gold nanorod ensembles as artificial molecules for applications in sensors. J. Mater. Chem. **21**, 16759–16782 (2011)
154. H. Ko, S. Singamaneni, V.V. Tsukruk, Nanostructured surfaces and assemblies as SERS media. Small **4**, 1576–1599 (2008)
155. M. Gluodenis, C.A. Foss, The effect of mutual orientation on the spectra of metal nanoparticle rod-rod and rod-sphere pairs. J. Phys. Chem. B **106**, 9484–9489 (2002)
156. B. Nikoobakht, J.P. Wang, M.A. El-Sayed, Surface-enhanced Raman scattering of molecules adsorbed on gold nanorods: off-surface plasmon resonance condition. Chem. Phys. Lett. **366**, 17–23 (2002)
157. X. Huang, I.H. El-Sayed, W. Qian, M.A. El-Sayed, Cancer cells assemble and align gold nanorods conjugated to antibodies to produce highly enhanced, sharp, and polarized surface Raman spectra: a potential cancer diagnostic marker. Nano Lett. **7**, 1591–1597 (2007)
158. S.W. Bishnoi, C.J. Rozell, C.S. Levin, M.K. Gheith, B.R. Johnson, D.H. Johnson, N. J. Halas, All-optical nanoscale pH meter. Nano Lett. **6**, 1687–1692 (2006)
159. C.M. Xue, Y.Q. Xu, Y. Pang, D.S. Yu, L.M. Dai, M. Gao, A. Urbas, Q. Li, Organo-soluble porphyrin mixed monolayer-protected gold nanorods with intercalated fullerenes. Langmuir **28**, 5956–5963 (2012)
160. C.M. Xue, O. Birel, M. Gao, S. Zhang, L.M. Dai, A. Urbas, Q. Li, Perylene monolayer protected gold nanorods: unique optical, electronic properties and self-assemblies. J. Phys. Chem. C **116**, 10396–10404 (2012)
161. C.M. Xue, Y.H. Xue, L.M. Dai, A. Urbas, Q. Li, Size- and shape-dependent fluorescence quenching of gold nanoparticles on perylene dye. Adv. Opt. Mater. **1**, 581–587 (2013)
162. R. Bardhan, S. Lal, A. Joshi, N.J. Halas, Theranostic nanoshells: from probe design to imaging and treatment of cancer. Acc. Chem. Res. **44**, 936–946 (2011)
163. E. Boisselier, D. Astruc, Gold nanoparticles in nanomedicine: preparations, imaging, diagnostics, therapies and toxicity. Chem. Soc. Rev. **38**, 1759–1782 (2009)
164. A.M. Alkilany, P.K. Nagaria, C.R. Hexel, T.J. Shaw, C.J. Murphy, M.D. Wyatt, Cellular uptake and cytotoxicity of gold nanorods: molecular origin of cytotoxicity and surface effects. Small **5**, 701–708 (2009)
165. Y.-S. Chen, Y.-C. Hung, I. Liau, G.S. Huang, Assessment of the in vivo toxicity of gold nanoparticles. Nanoscale Res. Lett. **4**, 858–864 (2009)
166. A.M. Alkilany, C.J. Murphy, Toxicity and cellular uptake of gold nanoparticles: what we have learned so far? J. Nanopart. Res. **12**, 2313–2333 (2010)
167. X.L. Zhou, J.M. El Khoury, L.T. Qu, L.M. Dai, Q. Li, A facile synthesis of aliphatic thiol surfactant with tunable length as a stabilizer of gold nanoparticles in organic solvents. J. Colloid Interface Sci. **308**, 381–384 (2007)
168. J.M. El Khoury, X.L. Zhou, L.T. Qu, L.M. Dai, A. Urbas, Q. Li, Organo-soluble photoresponsive azo thiol monolayer-protected gold nanorods. Chem. Commun. **16**, 2109–2111 (2009)
169. Y. Li, D. Yu, L. Dai, A. Urbas, Q. Li, Organo-soluble chiral thiol-monolayer-protected gold nanorods. Langmuir **27**, 98–103 (2011)
170. J.W. Hotchkiss, A.B. Lowe, S.G. Boyes, Surface modification of gold nanorods with polymers synthesized by reversible addition-fragmentation chain transfer polymerization. Chem. Mater. **19**, 6–13 (2007)
171. K. Liu, Z.H. Nie, N.N. Zhao, W. Li, M. Rubinstein, E. Kumacheva, Step-growth polymerization of inorganic nanoparticles. Science **329**, 197–200 (2010)

172. A. Gole, C.J. Murphy, Polyelectrolyte-coated gold nanorods: synthesis, characterization and immobilization. Chem. Mater. **17**, 1325–1330 (2005)
173. J.Y. Huang, K.S. Jackson, C.J. Murphy, Polyelectrolyte wrapping layers control rates of photothermal molecular release from gold nanorods. Nano Lett. **12**, 2982–2987 (2012)
174. E.E. Connor, J. Mwamuka, A. Gole, C.J. Murphy, M.D. Wyatt, Gold nanoparticles are taken up by human cells but do not cause acute cytotoxicity. Small **1**, 325–327 (2005)
175. H. Takahashi, Y. Niidome, T. Niidome, K. Kaneko, H. Kawasaki, S. Yamada, Modification of gold nanorods using phospatidylcholine to reduce cytotoxicity. Langmuir **22**, 2–5 (2006)
176. T.S. Hauck, A.A. Ghazani, W.C.W. Chan, Assessing the effect of surface chemistry on gold nanorod uptake, toxicity, and gene expression in mammalian cells. Small **4**, 153–159 (2008)
177. T. Niidome, M. Yamagata, Y. Okamoto, Y. Akiyama, H. Takahashi, T. Kawano, Y. Katayama, Y. Niidome, PEG-modified gold nanorods with a stealth character for in vivo applications. J. Control. Release **114**, 343–347 (2006)
178. Q. Dai, J. Coutts, J.H. Zou, Q. Huo, Surface modification of gold nanorods through a place exchange reaction inside an ionic exchange resin. Chem. Commun. **25**, 2858–2860 (2008)
179. Z.Y. Tang, Z.L. Zhang, Y. Wang, S.C. Glotzer, N.A. Kotov, Self-assembly of CdTe nanocrystals into free-floating sheets. Science **314**, 274–278 (2006)
180. K.J. Stebe, E. Lewandowski, M. Ghosh, Oriented assembly of metamaterials. Science **325**, 159–160 (2009)
181. E. Dujardin, L.B. Hsin, C.R.C. Wang, S. Mann, DNA-driven self-assembly of gold nanorods. Chem. Commun. **14**, 1264–1265 (2001)
182. T.S. Sreeprasad, A.K. Samal, T. Pradeep, One-, two-, and three-dimensional superstructures of gold nanorods induced by dimercaptosuccinic acid. Langmuir **24**, 4589–4599 (2008)
183. K. Mitamura, T. Imae, N. Saito, O. Takai, Fabrication and self-assembly of hydrophobic gold nanorods. J. Phys. Chem. B **111**, 8891–8898 (2007)
184. J.Y. Chang, H.M. Wu, H. Chen, Y.C. Ling, W.H. Tan, Oriented assembly of Au nanorods using biorecognition system. Chem. Commun. **8**, 1092–1094 (2005)
185. B. Pan, D. Cui, C. Ozkan, P. Xu, T. Huang, Q. Li, H. Chen, F. Liu, F. Gao, R. He, DNA-Templated ordered array of gold nanorods in one and two dimensions. J. Phys. Chem. C **111**, 12572–12576 (2007)
186. C.J. Orendorff, P.L. Hankins, C.J. Murphy, pH-triggered assembly of gold nanorods. Langmuir **21**, 2022–2026 (2005)
187. P.K. Jain, S. Eustis, M.A. El-Sayed, Plasmon coupling in nanorod assemblies: optical absorption, discrete dipole approximation simulation, and exciton-coupling model. J. Phys. Chem. B **110**, 18243–18253 (2006)
188. A. Guerrero-Martinez, J. Perez-Juste, E. Carbo-Argibay, G. Tardajos, L.M. Liz-Marzan, Gemini-surfactant-directed self-assembly of monodisperse gold nanorods into standing superlattices. Angew. Chem. Int. Ed. **48**, 9484–9488 (2009)
189. S. Gomez-Grana, J. Perez-Juste, R.A. Alvarez-Puebla, A. Guerrero-Martinez, L.M. Liz-Marzan, Self-assembly of Au@Ag nanorods mediated by gemini surfactants for highly efficient SERS-active supercrystals. Adv. Opt. Mater. **1**, 477–481 (2013)
190. M.J.A. Hore, R.J. Composto, Nanorod self-assembly for tuning optical absorption. ACS Nano **4**, 6941–6949 (2010)
191. J. Perez-Juste, B. Rodriguez-Gonzalez, P. Mulvaney, L.M. Liz-Marzan, Optical control and patterning of gold-nanorod-poly(vinyl alcohol) nanocomposite films. Adv. Funct. Mater. **15**, 1065–1071 (2005)
192. B.M.I. van der Zande, G.J.M. Koper, H.N.W. Lekkerkerker, Alignment of rod-shaped gold particles by electric fields. J. Phys. Chem. B **103**, 5754–5760 (1999)
193. A.B. Golovin, O.D. Lavrentovich, Electrically reconfigurable optical metamaterial based on colloidal dispersion of metal nanorods in dielectric fluid. Appl. Phys. Lett. **95**, 254104 (2009)
194. Q. Liu, Y. Cui, D. Gardner, X. Li, S. He, I.I. Smalyukh, Self-alignment of plasmonic gold nanorods in reconfigurable anisotropic fluids for tunable bulk metamaterial applications. Nano Lett. **10**, 1347–1353 (2010)

195. C. Xue, K. Gutierrez-Cuevas, M. Gao, A. Urbas, Q. Li, Photomodulated self-assembly of hydrophobic thiol monolayer-protected gold nanorods and their alignment in thermotropic liquid crystal. J. Phys. Chem. C **117**, 21603–21608 (2013)
196. G.Q. Jiang, M.J.A. Hore, S. Gam, R.J. Composto, Gold nanorods dispersed in homopolymer films: optical properties controlled by self-assembly and percolation of nanorods. ACS Nano **6**, 1578–1588 (2012)
197. M. Das, N. Sanson, D. Fava, E. Kumacheva, Microgels loaded with gold nanorods: photothermally triggered volume transitions under physiological conditions. Langmuir **23**, 196–201 (2007)
198. M. Karg, I. Pastoriza-Santos, J. Perez-Juste, T. Hellweg, L.M. Liz-Marzan, Nanorod coated PNIPAM microgels: thermoresponsive optical properties. Small **3**, 1222–1229 (2007)
199. C.L. Murphy, C.J. Orendorff, Alignment of gold nanorods in polymer composites and on polymer surfaces. Adv. Mater. **17**, 2173–2177 (2005)
200. R.D. Deshmukh, Y. Liu, R.J. Composto, Two-dimensional confinement of nanorods in block copolymer domains. Nano Lett. **7**, 3662–3668 (2007)
201. D. Nepal, M.S. Onses, K. Park, M. Jespersen, C.J. Thode, P.F. Nealey, R.A. Vaia, Control over position, orientation, and spacing of arrays of gold nanorods using chemically nanopatterned surfaces and tailored particle-particle-surface interactions. ACS Nano **6**, 5693–5701 (2012)
202. L. Vigderman, B.P. Khanal, E.R. Zubarev, Functional gold nanorods: synthesis, self-assembly, and sensing applications. Adv. Mater. **24**, 4811–4841 (2012)
203. G. Schmid, Large clusters and colloids-metals in the embryonic state. Chem. Rev. **92**, 1709–1727 (1992)
204. M. Haruta, N. Yamada, T. Kobayashi, S. Iijima, Gold catalysts prepared by coprecipitation for low-temperature oxidation of hydrogen and of carbon-monoxide. J. Catal. **115**, 301–309 (1989)
205. Y. Kuwauchi, H. Yoshida, T. Akita, M. Haruta, S. Takeda, Intrinsic catalytic structure of gold nanoparticles supported on TiO_2. Angew. Chem. Int. Ed. **51**, 7729–7733 (2012)
206. R. Narayanan, M.A. El-Sayed, Catalysis with transition metal nanoparticles in colloidal solution: nanoparticle shape dependence and stability. J. Phys. Chem. B **109**, 12663–12676 (2005)
207. M.A. Sanchez-Castillo, C. Couto, W.B. Kim, J.A. Dumesic, Gold-nanotube membranes for the oxidation of CO at gas-water interfaces. Angew. Chem. Int. Ed. **43**, 1140–1142 (2004)
208. P. Li, Z. Wei, T. Wu, Q. Peng, Y. Li, Au-ZnO hybrid nanopyramids and their photocatalytic properties. J. Am. Chem. Soc. **133**, 5660–5663 (2011)
209. X. Cui, C. Zhang, F. Shi, Y. Deng, Au/Ag-Mo nano-rods catalyzed reductive coupling of nitrobenzenes and alcohols using glycerol as the hydrogen source. Chem. Commun. **48**, 9391–9393 (2012)
210. M. Stratakis, H. Garcia, Catalysis by supported gold nanoparticles: beyond aerobic oxidative processes. Chem. Rev. **112**, 4469–4506 (2012)
211. K. Aslan, J.R. Lakowicz, C.D. Geddes, Plasmon light scattering in biology and medicine: new sensing approaches, visions and perspectives. Curr. Opin. Chem. Biol. **9**, 538–544 (2005)
212. C. Novo, A.M. Funston, P. Mulvaney, Direct observation of chemical reactions on single gold nanocrystals using surface plasmon spectroscopy. Nat. Nanotechnol. **3**, 598–602 (2008)
213. G.J. Nusz, S.M. Marinakos, A.C. Curry, A. Dahlin, F. Hook, A. Wax, A. Chilkoti, Label-free plasmonic detection of biomolecular binding by a single gold nanorod. Anal. Chem. **80**, 984–989 (2008)
214. C.J. Murphy, A.M. Gole, S.E. Hunyadi, J.W. Stone, P.N. Sisco, A. Alkilany, B.E. Kinard, P. Hankins, Chemical sensing and imaging with metallic nanorods. Chem. Commun. **5**, 544–557 (2008)
215. C. Yu, J. Irudayaraj, Quantitative evaluation of sensitivity and selectivity of multiplex nanoSPR biosensor assays. Biophys. J. **93**, 3684–3692 (2007)

216. J. York, D. Spetzler, F.S. Xiong, W.D. Frasch, Single-molecule detection of DNA via sequence-specific links between F-1-ATPase motors and gold nanorod sensors. Lab Chip **8**, 415–419 (2008)
217. N.R. Jana, T. Pal, Anisotropic metal nanoparticles for use as surface-enhanced Raman substrates. Adv. Mater. **19**, 1761–1765 (2007)
218. X.M. Qian, X.H. Peng, D.O. Ansari, Q. Yin-Goen, G.Z. Chen, D.M. Shin, L. Yang, A.N. Young, M.D. Wang, S.M. Nie, In vivo tumor targeting and spectroscopic detection with surface-enhanced Raman nanoparticle tags. Nat. Biotechnol. **26**, 83–90 (2008)
219. A.K. Oyelere, P.C. Chen, X.H. Huang, I.H. El-Sayed, M.A. El-Sayed, Peptide-conjugated gold nanorods for nuclear targeting. Bioconjugate Chem. **18**, 1490–1497 (2007)
220. N. Bi, Y. Chen, H. Qi, X. Zheng, Y. Chen, X. Liao, H. Zhang, Y. Tian, Spectrophotometric determination of mercury(II) ion using gold nanorod as probe. Sensor. Actuat. B-Chem. **166**, 766–771 (2012)
221. F.-M. Li, J.-M. Liu, X.-X. Wang, L.-P. Lin, W.-L. Cai, X. Lin, Y.-N. Zeng, Z.-M. Li, S.-Q. Lin, Non-aggregation based label free colorimetric sensor for the detection of Cr (VI) based on selective etching of gold nanorods. Sensor. Actuat. B-Chem. **155**, 817–822 (2011)
222. G. Chen, Y. Jin, L. Wang, J. Deng, C. Zhang, Gold nanorods-based FRET assay for ultrasensitive detection of Hg^{2+}. Chem. Commun. **47**, 12500–12502 (2011)
223. S.M. Yoo, T. Kang, H. Kang, H. Lee, M. Kang, S.Y. Lee, B. Kim, Combining a nanowire SERS sensor and a target recycling reaction for ultrasensitive and multiplex identification of pathogenic fungi. Small **7**, 3371–3376 (2011)
224. E.C. Dreaden, M.A. El-Sayed, Detecting and destroying cancer cells in more than one way with noble metals and different confinement properties on the nanoscale. Acc. Chem. Res. **45**, 1854–1865 (2012)
225. L. Wu, Z. Wang, S. Zong, Z. Huang, P. Zhang, Y. Cui, A SERS-based immunoassay with highly increased sensitivity using gold/silver core-shell nanorods. Biosens. Bioelectron. **38**, 94–99 (2012)
226. Z. Siwy, L. Trofin, P. Kohli, L.A. Baker, C. Trautmann, C.R. Martin, Protein biosensors based on biofunctionalized conical gold nanotubes. J. Am. Chem. Soc. **127**, 5000–5001 (2005)
227. G. Lin, W. Lu, W. Cui, L. Jiang, A simple synthesis method for gold nano- and microplate fabrication using a tree-type multiple-amine head surfactant. Cryst. Growth Des. **10**, 1118–1123 (2010)
228. P. Pienpinijtham, X.X. Han, T. Suzuki, C. Thammacharoen, S. Ekgasit, Y. Ozaki, Micrometer-sized gold nanoplates: starch-mediated photochemical reduction synthesis and possibility of application to tip-enhanced Raman scattering (TERS). Phys. Chem. Chem. Phys. **14**, 9636–9641 (2012)
229. C. Loo, A. Lowery, N.J. Halas, J. West, R. Drezek, Immunotargeted nanoshells for integrated cancer imaging and therapy. Nano Lett. **5**, 709–711 (2005)
230. L.R. Hirsch, J.B. Jackson, A. Lee, N.J. Halas, J. West, A whole blood immunoassay using gold nanoshells. Anal. Chem. **75**, 2377–2381 (2003)
231. A.M. Gobin, M.H. Lee, N.J. Halas, W.D. James, R.A. Drezek, J.L. West, Near-infrared resonant nanoshells for combined optical imaging and photothermal cancer therapy. Nano Lett. **7**, 1929–1934 (2007)
232. M.A. Mahmoud, M.A. El-Sayed, Time dependence and signs of the shift of the surface plasmon resonance frequency in nanocages elucidate the nanocatalysis mechanism in hollow nanoparticles. Nano Lett. **11**, 946–953 (2011)
233. S.A. Khan, R. Kanchanapally, Z. Fan, L. Beqa, A.K. Singh, D. Senapati, P.C. Ray, A gold nanocage-CNT hybrid for targeted imaging and photothermal destruction of cancer cells. Chem. Commun. **48**, 6711–6713 (2012)
234. M.H. Rashid, R.R. Bhattacharjee, T.K. Mandal, Organic ligand-mediated synthesis of shape-tunable gold nanoparticles: an application of their thin film as refractive index sensors. J. Phys. Chem. C **111**, 9684–9693 (2007)

235. Y. Zhu, H. Kuang, L. Xu, W. Ma, C. Peng, Y. Hua, L. Wang, C. Xu, Gold nanorod assembly based approach to toxin detection by SERS. J. Mater. Chem. **22**, 2387–2391 (2012)
236. Y.B. Mollamahalle, M. Ghorbani, A. Dolati, Electrodeposition of long gold nanotubes in polycarbonate templates as highly sensitive 3D nanoelectrode ensembles. Electrochim. Acta **75**, 157–163 (2012)
237. R. Mout, D.F. Moyano, S. Rana, V.M. Rotello, Surface functionalization of nanoparticles for nanomedicine. Chem. Soc. Rev. **41**, 2539–2544 (2012)
238. S.E. Lee, D.Y. Sasaki, T.D. Perroud, D. Yoo, K.D. Patel, L.P. Lee, Biologically functional cationic phospholipid-gold nanoplasmonic carriers of RNA. J. Am. Chem. Soc. **131**, 14066–14074 (2009)
239. K. Kim, S.-W. Huang, S. Ashkenazi, M. O'Donnell, A. Agarwal, N.A. Kotov, M.F. Denny, M.J. Kaplan, Photoacoustic imaging of early inflammatory response using gold nanorods. Appl. Phys. Lett. **90**, 223901 (2007)
240. D.L. Chamberland, A. Agarwal, N. Kotov, J.B. Fowlkes, P.L. Carson, X. Wang, Photoacoustic tomography of joints aided by an Etanercept-conjugated gold nanoparticle contrast agent—an ex vivo preliminary rat study. Nanotechnology **19**, 095101 (2008)
241. A. Agarwal, S.W. Huang, M. O'Donnell, K.C. Day, M. Day, N. Kotov, S. Ashkenazi, Targeted gold nanorod contrast agent for prostate cancer detection by photoacoustic imaging. Appl. Phys. Lett. **102**, 064701 (2007)
242. C. Loo, L. Hirsch, M.H. Lee, E. Chang, J. West, N.J. Halas, R. Drezek, Gold nanoshell bioconjugates for molecular imaging in living cells. Opt. Lett. **30**, 1012–1014 (2005)
243. X. Yang, S.E. Skrabalak, Z.-Y. Li, Y. Xia, L.V. Wang, Photoacoustic tomography of a rat cerebral cortex in vivo with au nanocages as an optical contrast agent. Nano Lett. **7**, 3798–3802 (2007)
244. R. Huschka, J. Zuloaga, M.W. Knight, L.V. Brown, P. Nordlander, N.J. Halas, Light-induced release of DNA from gold nanoparticles: nanoshells and nanorods. J. Am. Chem. Soc. **133**, 12247–12255 (2011)
245. C. Loo, A. Lin, L. Hirsch, M.H. Lee, J. Barton, N.J. Halas, J. West, R. Drezek, Nanoshell-enabled photonics-based imaging and therapy of cancer. Tech. Canc. Res. Treat. **3**, 33–40 (2004)
246. J. You, R. Zhang, G. Zhang, M. Zhong, Y. Liu, C.S. Van Pelt, D. Liang, W. Wei, A.K. Sood, C. Li, Photothermal-chemotherapy with doxorubicin-loaded hollow gold nanospheres: a platform for near-infrared light-trigged drug release. J. Control. Release **158**, 319–328 (2012)
247. L.R. Hirsch, R.J. Stafford, J.A. Bankson, S.R. Sershen, B. Rivera, R.E. Price, J.D. Hazle, N. J. Halas, J.L. West, Nanoshell-mediated near-infrared thermal therapy of tumors under magnetic resonance guidance. Proc. Natl. Acad. Sci. USA **100**, 13549–13554 (2003)
248. E.C. Dreaden, S.C. Mwakwari, L.A. Austin, M.J. Kieffer, A.K. Oyelere, M.A. El-Sayed, Small molecule-gold nanorod conjugates selectively target and induce macrophage cytotoxicity towards breast cancer cells. Small **8**, 2819–2822 (2012)
249. E.B. Dickerson, E.C. Dreaden, X.H. Huang, I.H. El-Sayed, H.H. Chu, S. Pushpanketh, J.F. McDonald, M.A. El-Sayed, Gold nanorod assisted near-infrared plasmonic photothermal therapy (PPTT) of squamous cell carcinoma in mice. Cancer Lett. **269**, 57–66 (2008)
250. D. Pissuwan, S.M. Valenzuela, M.C. Killingsworth, X.D. Xu, M.B. Cortie, Targeted destruction of murine macrophage cells with bioconjugated gold nanorods. J. Nanopart. Res. **9**, 1109–1124 (2007)
251. H. Takahashi, T. Niidome, A. Nariai, Y. Niidome, S. Yamada, Photothermal reshaping of gold nanorods prevents further cell death. Nanotechnology **17**, 4431–4435 (2006)
252. L.C. Kennedy, L.R. Bickford, N.A. Lewinski, A.J. Coughlin, Y. Hu, E.S. Day, J.L. West, R. A. Drezek, A new era for cancer treatment: gold-nanoparticle-mediated thermal therapies. Small **7**, 169–183 (2011)
253. J. Chen, D. Wang, J. Xi, L. Au, A. Siekkinen, A. Warsen, Z.-Y. Li, H. Zhang, Y. Xia, X. Li, Immuno gold nanocages with tailored optical properties for targeted photothermal destruction of cancer cells. Nano Lett. **7**, 1318–1322 (2007)

254. F. Tielens, J. Andres, Prediction of gold zigzag nanotube-like structure based on Au_{32} units: a quantum chemical study. J. Phys. Chem. C **111**, 10342–10346 (2007)
255. Y. Horiguchi, T. Niidome, S. Yamada, N. Nakashima, Y. Niidome, Expression of plasmid DNA released from DNA conjugates of gold nanorods. Chem. Lett. **36**, 952–953 (2007)
256. L. Dykman, N. Khlebtsov, Gold nanoparticles in biomedical applications: recent advances and perspectives. Chem. Soc. Rev. **41**, 2256–2282 (2012)
257. C.C. Chen, Y.P. Lin, C.W. Wang, H.C. Tzeng, C.H. Wu, Y.C. Chen, C.P. Chen, L.C. Chen, Y.C. Wu, DNA-gold nanorod conjugates for remote control of localized gene expression by near infrared irradiation. J. Am. Chem. Soc. **128**, 3709–3715 (2006)
258. H. Takahashi, Y. Niidome, S. Yamada, Controlled release of plasmid DNA from gold nanorods induced by pulsed near-infrared light. Chem. Commun. **17**, 2247–2249 (2005)
259. I. Gorelikov, L.M. Field, E. Kumacheva, Hybrid microgels photoresponsive in the near-infrared spectral range. J. Am. Chem. Soc. **126**, 15938–15939 (2004)
260. A. Shiotani, T. Mori, T. Niidome, Y. Niidome, Y. Katayama, Stable incorporation of gold nanorods into N-isopropylacrylamide hydrogels and their rapid shrinkage induced by near-infrared laser irradiation. Langmuir **23**, 4012–4018 (2007)
261. Q. Wei, J. Ji, J. Shen, Synthesis of near-infrared responsive gold nanorod/PNIPAAm core/shell nanohybrids via surface initiated ATRP for smart drug delivery. Macromol. Rapid Commun. **29**, 645–650 (2008)
262. A. Barhoumi, R. Huschka, R. Bardhan, M.W. Knight, N.J. Halas, Light-induced release of DNA from plasmon-resonant nanoparticles: Towards light-controlled gene therapy. Chem. Phys. Lett. **482**, 171–179 (2009)
263. R. Huschka, O. Neumann, A. Barhoumi, N.J. Halas, Visualizing light-triggered release of molecules inside living cells. Nano Lett. **10**, 4117–4122 (2010)
264. W. Chen, R. Bardhan, M. Bartels, C. Perez-Torres, R.G. Pautler, N.J. Halas, A. Joshi, A molecularly targeted theranostic probe for ovarian cancer. Mol. Cancer Ther. **9**, 1028–1038 (2010)
265. M.S. Yavuz, Y.Y. Cheng, J.Y. Chen, C.M. Cobley, Q. Zhang, M. Rycenga, J.W. Xie, C. Kim, K.H. Song, A.G. Schwartz, L.H.V. Wang, Y.N. Xia, Gold nanocages covered by smart polymers for controlled release with near-infrared light. Nat. Mater. **8**, 935–939 (2009)
266. W. Li, X. Cai, C. Kim, G. Sun, Y. Zhang, R. Deng, M. Yang, J. Chen, S. Achilefu, L.V. Wang, Y. Xia, Gold nanocages covered with thermally-responsive polymers for controlled release by high-intensity focused ultrasound. Nanoscale **3**, 1724–1730 (2011)
267. W. Wang, T. Yan, S. Cui, J. Wan, A bioresponsive controlled-release biosensor using Au nanocages capped with an aptamer-based molecular gate and its application in living cells. Chem. Commun. **48**, 10228–10230 (2012)
268. E. Hao, G.C. Schatz, Electromagnetic fields around silver nanoparticles and dimers. J. Chem. Phys. **120**, 357–366 (2004)
269. J.-M. Lamarre, F. Billard, C.H. Kerboua, M. Lequime, S. Roorda, L. Martinu, Anisotropic nonlinear optical absorption of gold nanorods in a silica matrix. Opt. Commun. **281**, 331–340 (2008)
270. W. Cai, U.K. Chettiar, A.V. Kildishev, V.M. Shalaev, Optical cloaking with metamaterials. Nat. Photon. **1**, 224–227 (2007)
271. S. Nah, L. Li, R. Liu, J. Hao, S.B. Lee, J.T. Fourkas, Metal-enhanced multiphoton absorption polymerization with gold nanowires. J. Phys. Chem. C **114**, 7774–7779 (2010)
272. S. Lal, J.H. Hafner, N.J. Halas, S. Link, P. Nordlander, Noble metal nanowires: from plasmon waveguides to passive and active devices. Acc. Chem. Res. **45**, 1887–1895 (2012)
273. C.L. Nehl, J.H. Hafner, Shape-dependent plasmon resonances of gold nanoparticles. J. Mater. Chem. **18**, 2415–2419 (2008)